U-Pb ZIRCON CONSTRAINTS ON THE TECTONIC EVOLUTION OF SOUTHEASTERN TIBET, NAMCHE BARWA AREA

AMANDA L. BOOTH*, PETER K. ZEITLER**, WILLIAM S.F. KIDD***,
JOSEPH WOODEN****, YUPING LIU*****, BRUCE IDLEMAN**,
MICHAEL HREN*, and C. PAGE CHAMBERLAIN*

ABSTRACT.   The eastern syntaxis of the Himalayas is expressed in the crust as a pronounced southward bend in the orogen. The change in strike of geologic features coincides with the high topography of the Namche Barwa region, the exposure of granulite-grade metamorphic rocks, and a 180-degree bend in the Yalu Tsangpo. We have conducted a geochronologic and geochemical investigation of several suites of granitoids collected from the Namche Barwa massif and subjacent terranes of southeastern Tibet, ranging from cm-scale dikes and sills to larger, outcrop-scale intrusions. U-Pb SHRIMP-RG zircon ages establish at least five magmatic episodes: ~400 to 500 Ma, ~120 Ma, 40 to 70 Ma, 18 to 25 Ma, and 3 to 10 Ma. These episodes broadly correlate to spatial patterns in sample localities, as follows: 400 to 500 Ma ages occur in zircon cores collected from within the massif proper; ~120 Ma granites, related to early Gangdese arc plutonism, are primarily located northeast of Namche Barwa; later (40 - 70 Ma) Gangdese activity is expressed in granites west of Namche Barwa. 18 to 25 Ma granites occur both along the suture zone west of Gyala Peri, and directly north of Namche Barwa along the area of the Jiali fault zone, and are attributed both to shearing within the Jiali fault zone and to an early Miocene Gangdese Thrust event. Exceptionally young (<10 Ma) zircon ages are clustered near the core of the massif, along the Yalu Tsangpo gorge. Trace-element geochemical data indicates the presence of both fluid-present and fluid absent melts, with a fluid-absent (decompression) melting regime dominating near the core of Namche Barwa.

INTRODUCTION

Spatial and temporal patterns among Himalayan granites have been critical for reconstructing the tectonic framework of the India-Asia collision. Granite production and emplacement can be indicative of numerous different lithospheric melting regimes dominating within an area, such as decompression melting, shear heating, dehydration melting, *et cetera* (for example, Le Fort, 1975, 1981; Debon and others, 1985; Le Fort and others, 1987; Zeitler and Chamberlain, 1991; Harris and Massey, 1994; Scaillet and others, 1995; Harrison and others, 1998). Tectonic processes attributed with producing Himalayan crustal melts include syn-orogenic extension (Molnar and others, 1993; Fielding, 1996; Edwards and Harrison, 1997; Harrison and others, 1997a; Murphy and Harrison, 1999), fluxing by volatiles during thrusting along the Main Central Thrust (Le Fort, 1981; Le Fort and others, 1987), decompression melting during rapid denudation (Zeitler and others, 1993; Winslow and others, 1995; Whittington and Treloar, 2002), slab break-off (Miller and others, 1999; Chemenda and others, 2000; Yin and Harrison, 2000; Maheo and others, 2002; Kohn and Parkinson, 2002), continental subduction (Meyer and others, 1998; Wang and others, 2001), slab roll-back (Ding and others, 2003), slab detachment (Kosarev and others, 1999; Tilman and others, 2003), and subduction of remnant oceanic lithosphere (Murphy and Yin, 2003). Shear heating during strike-slip motion along the Red River

*Department of Geological and Environmental Sciences, Bldg. 320, Stanford University, Stanford, California, 94305; mbooth@pangea.stanford.edu
**Department of Earth and Environmental Sciences, Lehigh University, Bethlehem, Pennsylvania, 18015
***Department of Earth and Atmospheric Sciences, University at Albany, Albany, New York 12222
****U.S. Geological Survey, 345 Middlefield Road, Menlo Park, California 94025
*****Chengdu Institute of Geology and Mineral Sciences, Chengdu, China

fault, southeast of Tibet, has also been ascribed with producing partial melts (Schärer and others, 1994; Leloup and others, 1995).

Southeastern Tibet is an area that remains sparsely studied with respect to its tectonic evolution, particularly its deeper structure and igneous history. Many features, however, can be readily observed that suggest a complex series of tectono-magmatic events has helped to shape this region, including: (1) The eastern syntaxis is expressed in the crust as a clear bend in the topographic, structural, and geological trends, particularly the Indus-Tsangpo Suture Zone (ITSZ) and the High Himalayan Crystalline belt; and (2) Embedded within the eastern syntaxis is an antiformal basement massif, Namche Barwa, where the deep gorge of the Yalu Tsangpo exposes ~7000 meters of actively deforming metamorphic rocks and granites as young as Pleistocene in age (Burg and others, 1997; Zeitler and others, 2001a).

This study deals with granitic melts present on a variety of scales in the eastern Himalayan syntaxis and southeastern Tibet. The results of our study suggest a complex tectonic history for southeastern Tibet, including at least five magmatic episodes and the production of both fluid-saturated and undersaturated melts.

GEOLOGIC AND TECTONIC OVERVIEW

An important element of understanding the tectonics of Southeast Asia is tracing the assembly of Tibet itself. Tibet proper consists of terranes accreted successively to the southern margin of Eurasia (Dewey and others, 1988; Murphy and others, 1997; Yin and Harrison, 2000; Kapp and others, 2003a, 2003b). The southernmost of these terranes is the Lhasa block, which originated by rifting from Gondwana in the late Paleozoic and was sutured to Asia by a late Jurassic-early Cretaceous collision (~140 Ma). Subsequently, the southern Lhasa block was the site of an Andean-type magmatic arc until the India-Asia collision began in the Eocene. To the south, the Lhasa block is separated from rocks of Indian affinity in the Tethyan Himalaya by the ophiolitic ITSZ. The suture has been structurally modified, most likely by the south-directed Gangdese Thrust System (GTS; Yin and others, 1994; Harrison and others, 2000) and by back thrusts of the north directed Renbu Zedong Thrust System (RZTS; Yin and others, 1994, 1999; Ratschbacher and others, 1994; Quidelleur and others, 1997). Some workers, however, have interpreted the Gangdese thrust to be an unconformity, rather than an actual structure (that is, Aitchison and others, 2003).

The eastern Himalayan syntaxis represents a broad region over which structural trends in southeastern Tibet and the Himalayan orogen turn from E-W to N-S striking. This syntaxis is also evident in the trends of surface features such as major river valleys located along strike-slip faults (Hallet and Molnar, 2001), and overall the syntaxis likely reflects several generations of structural events along the eastern edge of the Indian plate, including Miocene extrusion tectonics (Wang and Burchfiel, 1997), and ongoing clockwise rotations (Burchfiel and others, 1998).

Near the peaks Namche Barwa and Gyala Peri, the eastern Himalayan syntaxis exposes both Indian and Asian continental components separated by a deformed ITSZ (fig. 1). The Gangdese or Transhimalayan Plutonic Belt (formerly part of the Asian plate margin) consists of Cretaceous and Paleogene calc-alkaline plutons intruded into Paleozoic and Mesozoic metasediments, and wraps around the antiformal Namche Barwa metamorphic massif (Zhang and others, 1992; Burg and others, 1997). Around much of the syntaxis, a mylonitic zone separates the Transhimalayan rocks from the core of Indian basement gneisses. Serpentine lenses and abundant amphibolites within this zone suggest that this boundary is the eastern continuation of the ITSZ, with remnants of meta-ophiolites separating Asian from Indian plate rocks (Zhang and others, 1992; Burg and others, 1997). A distinctive belt of metasedimentary rocks (dominantly quartzites and pelites, with some calc-silicates), thought to be a more deformed and metamorphosed equivalent of the Tethyan Himalaya, also form part of
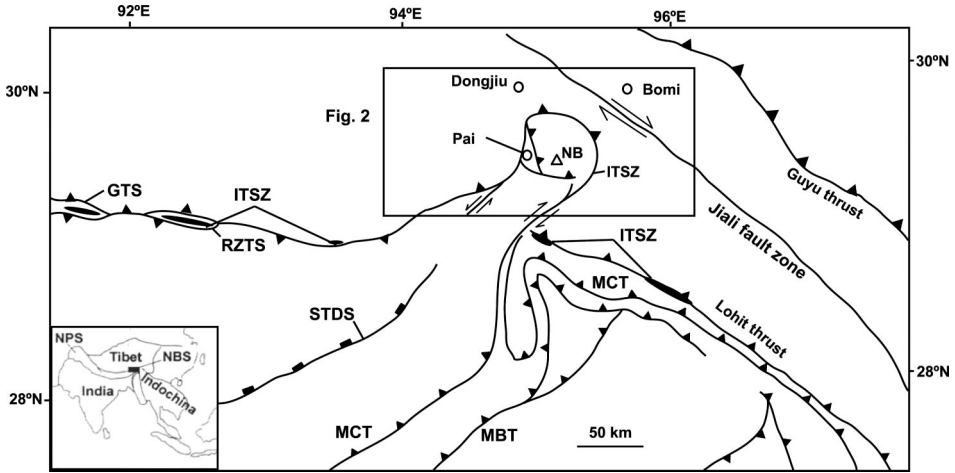
Fig. 1. Tectonic sketch map of southeastern Tibet, after Ding and others (2001). Location of fig. 2 shown in box. GTS = Gangdese Thrust System, RZTS = Renbu Zedong Thrust System, STDS = South Tibetan Detachment System, ITSZ = Indus Tsangpo Suture Zone, MCT = Main Central Thrust, MBT = Main Boundary Thrust, NB = Namche Barwa. Regional geographic location of Namche Barwa shown in inset. NBS = Namche Barwa Syntaxis, NPS = Nanga Parbat Syntaxis.

this zone of highly strained rocks. Medium to high-grade metamorphic rocks (presumably derived from Indian Basement rocks) make up the core of the syntaxis and were once structurally below the Transhimalayan Plutonic Belt. They are dominantly migmatitic gneisses of Proterozoic initial age (Zhang and others, 1992; Burg and others, 1997). According to Liu and Zhong (1997), they can be divided into a granulite group in the north and an amphibolite group in the south, with the former thrust over the latter by the Namula thrust system.

A number of granitoids with distinctly different means of formation occur within or near the eastern syntaxis. We briefly review the main types of granitoids that have been reported from the region to date.

Namche Barwa Massif.—In the core of this massif, granitic dikes and sills intrude Indian Basement gneisses on a range of scales. Burg and others (1998) reported leucogranite and pegmatite dikes in the Namche Barwa syntaxis, including leucosomes that crosscut metamorphic layering in the pelitic gneisses. This structural relationship indicates that anatexis has outlasted the main fabric development in the core of Namche Barwa. Single crystal U-Th-Pb analyses on zircon, xenotime and thorite by Burg and others (1997) provide leucosome crystallization ages ranging between 2.9 and 3.9 Ma, with a protolith age of 484 ± 3 Ma. Ding and others (2001) reported U-Pb zircon ages as young as ~11 Ma from mafic granulites and two-mica-bearing leucosomes within the massif's core. A cluster of ages at ~65 Ma likely crystallized during Andean-type Gangdese magmatism, while a younger (~40 Ma) cluster is interpreted to have crystallized during fluid-present, high-grade metamorphism during the early stages of India-Asia collision. The youngest, 11 to 25 Ma, zircon ages are attributed to a later high-grade metamorphic event, possibly related to decompression melting during rapid exhumation.

Nanga Parbat massif.—In the western Himalayan syntaxis, decompression melting has been invoked for the formation of leucogranites that intrude the Nanga Parbat massif (Zeitler and Chamberlain, 1991), due to the temporal coincidence of exhumation and melting. In addition to fluid-absent (decompression) melting, fluid-present melts have been documented at Nanga Parbat. The concurrence of both types of melt

reaction is attributed to a change from fluid-absent anatexis in the mid-crust (~20 km depth) to fluid infiltration in the upper crust (~10 km depth) (Whittington and others, 1999). These granites are among the youngest documented in the Himalayan system, at 1 to 3 Ma (Zeitler and Chamberlain, 1991).

Himalayan leucogranites.—Tertiary magmatism within the Himalaya proper is largely confined to two parallel granite belts, the High Himalayan Leucogranites and the North Himalayan Granites (Harrison and others, 1997b). A commonly prescribed model for Himalayan leucogranite genesis involves fluid advection from the dehydrating footwall into the relatively hot hanging wall, along major fault systems such as the Main Central Thrust (Le Fort, 1981; Le Fort and others, 1987). Improved knowledge of granite crystallization ages (Edwards and Harrison, 1997; Harrison and others, 1997a) suggests a different model, relating the formation of Miocene leucogranites to syn-orogenic extension on the South Tibetan Detachment System (STDS) around 20 Ma. This model assumes that the primary cause of melting is decompression during exhumation south of the STDS (Hodges and others, 1992; Harris and Massey, 1994). In southeastern Tibet, Miocene partial melts and late Eocene K-rich magmas have been attributed to simultaneous shear heating and rapid erosion (for example, Harrison and others, 1998) during coeval slip along the MCT and STDS. An alternative slab break-off model (Chemenda and others, 2000; Yin and Harrison, 2000; Kohn and Parkinson, 2002) has been proposed to explain the Miocene leucogranites, based on the occurrence of rare Eocene eclogites in southeastern Tibet. This model assumes subduction of Greater Himalayan crustal rocks to ~100 km depth in the Eocene followed by buoyant rise after decoupling from the mantle lithosphere.

Gangdese Arc.—Just to the north of the ITSZ is the Transhimalayan plutonic belt, a semi-continuous 2600-km-long batholith with rocks ranging in composition from gabbro to granite (Debon and others, 1986). In the proximity of the Namche Barwa syntaxis, this belt is represented by the Gangdese batholith, forming the root of the Gangdese magmatic arc that developed as a consequence of northward subduction of Neo-Tethys oceanic crust (Hodges, 2000, and references therein). Diorites and granodiorites from the eastern section of the Gangdese batholith yield geochronologic ages between 113 ± 2 Ma ($^{40}Ar/^{39}Ar$ method on amphiboles; Maluski and others, 1988) and 41.1 ± 0.4 Ma (U/Pb method on zircons; Schärer and others, 1984). There is a wide variety in composition (that is, Debon and others, 1986), but no clear relationship between chemistry and age of plutonism (Schärer and others, 1984).

Red River shear zone.—East of the Namche Barwa syntaxis, documented magmatism is associated with ductile deformation and high-grade metamorphism along the Red River shear zone (Schärer and others, 1990, 1994; Harrison and others, 1992; Leloup and Kienast, 1993; Leloup and others, 1993, 1995; Chung and others, 1998; Wang and others, 2001). Partial melts in the Red River shear zone coeval with ductile deformation yield ages of 22 to 23 Ma and geochemical data indicate anatexis at 20 to 15 km depth, with crustally derived mantle affinities (Zhang and Schärer, 1999).

Early Miocene melts, southern Tibet.—Two types of magmatism are documented in areas of southern Tibet from circa 25 to 10 Ma, those of ultrapotassic composition and of calc-alkaline composition (Coulon and others, 1986; Yin and others, 1994; Turner and others, 1996; Miller and others, 1999; Williams and others, 2001). These "postcollisional" magmas occur as small intrusive and extrusive bodies located west of Lhasa city. Recently, calc-alkaline magmas emplaced from circa 26 to 10 Ma have also been reported in the areas around Xigaze and east of Lhasa city (Chung and others, 2003), which exhibit geochemical signatures characteristic of adakites, lavas previously found only in subduction zones. Chung and others (2003) believe them to represent the first example of adakites produced in a modern continental collision setting, resulting from melting of thickened Tibetan lower crust, induced by removal of lithospheric

mantle in late Oligocene time. Murphy and Yin (2003), however, suggest that postcollision (Oligocene/Miocene) high-K, calc-alkaline magmatism along the southern margin of the Lhasa block may be attributed to late subduction of remnant Neo-Tethyan oceanic crust, producing magmatism.

Himalayan Paleozoic ages.—Le Fort and others (1980) first reported Paleozoic ages (516 ± 6 Ma; whole rock Rb/Sr method) on the Manshera granite in Pakistan. Recent work in the central Himalayas (Gehrels and others, 2003) also documents the existence of ~470 to 485 Ma granitic intrusions (U-Pb method on zircons) within Greater Himalayan metasediments, reflecting initiation of the Himalayan orogen along an early Paleozoic thrust belt. This age range is also supported by numerous ~480 to 500 Ma U-Pb zircon ages (Ferrara and others, 1983; Trivedi and others, 1984; Le Fort and others, 1986; Hodges and others, 1996; DeCelles and others, 1998, 2000; Miller and others, 2001) from cross-cutting granitic plutons and orthogneisses within Greater Himalayan rocks.

METHODS

Samples.—During September-October 2001 and May-June 2002 field seasons, our samples were gathered from five principal areas, and can be grouped as follows: [A] within the Namche Barwa massif (fig. 2) – from granitic dikes and migmatites intruding Indian plate gneisses and metasediments; [B] along the northwest margin of the Namche Barwa-Gyala Peri (NB-GP) massif – from granitic intrusions into both Lhasa block and Indian plate gneisses and metasediments; [C] substantially west of the NB-GP massif, spread out from Loulan toward Bayi, and along the Nyang River – intruding Lhasa block gneisses and metasediments; [D] north of Namche Barwa, along the inferred location of the Jiali Fault zone – from intrusions into Lhasa block gneisses and metasediments; and [E] northeast of Namche Barwa near the Jiali Fault zone – from presumed Gangdese plutonic rock of granodioritic compositions.

Group A samples, collected from within the Namche Barwa massif proper, are 20 to 300 cm-thick dikes and sills that intrude amphibolite to granulite grade Precambrian gneisses. Samples IG-2d, IG-4, and IG-6b were collected along the upper inner gorge of the Yalu Tsangpo (fig. 2), along a traverse from Jiala to Zhibei. Sample IG-2d (fig. 3) represents a deformed felsic melt pod within a 100-meter amphibolite section near Jiala. Sample IG-4 was collected from an ~3-meter leucocratic pegmatite dike that locally crosscuts and elsewhere is sheared concordantly into the foliation. Sample IG-6b was collected from a felsic crosscutting dikelet (~20 cm) within a small biotite gneiss outcrop exposed along the trail from Zhibei to Jiala, just northeast of Zhibei. Sample IG-15a was collected from a granitic sweat within the gneisses, along a road cut just to the east-northeast of Pai. Sample IG-16 was collected from a K-feldspar-bearing banded migmatite exposed along a jeep road from Pai to Duoxiong La, on the northwest side of Duoxiong La pass. Sample IG-18 was collected as float from an ~4 m, coarse-grained granitic boulder halfway to the top of Duoxiong La pass. The source of this boulder, however, was clearly from a large granite sill visible in the headwall above. We therefore justify the sampling of float in the case of IG-18, by asserting that the source rock is very well constrained.

Group B samples were collected along the northwestern margin of the NB-GP massif, and represent granite and pegmatite dikes intruding basement gneisses of both Lhasa block and Indian Plate origin. Samples BT-14, BT-15, BT-17 (fig. 4), BT-19, and BT-20 were collected from a section within the De'u Gungbu Valley (fig. 5), along an E-W traverse across the brittle-faulted western margin of the NB-GP massif (including the modified and very narrow Indus-Tsangpo suture zone). Within this group, BT-14 is a granitic gneiss, BT-15 represents a leucocratic pegmatite dike cross-cutting the Lhasa Block basement gneisses, BT-17 is a medium-grained granite dike from the westernmost edge of the Gyala Peri massif, cross-cutting the amphibolites near a brittle fault
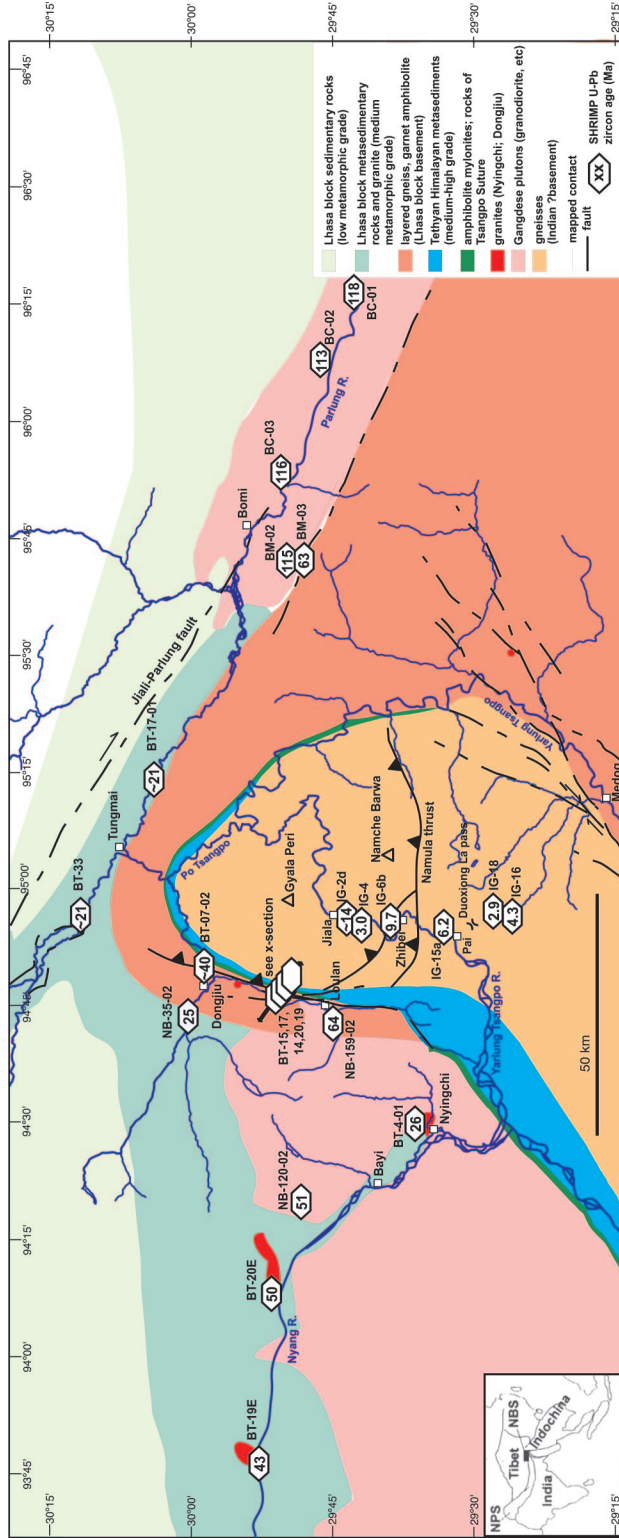
Fig. 2. Geological map of Namche Barwa syntaxis, showing major lithological units and faults, town names referred to in text, sample localities, and distribution of U-Pb zircon ages. Location of cross section (fig. 5) is shown.
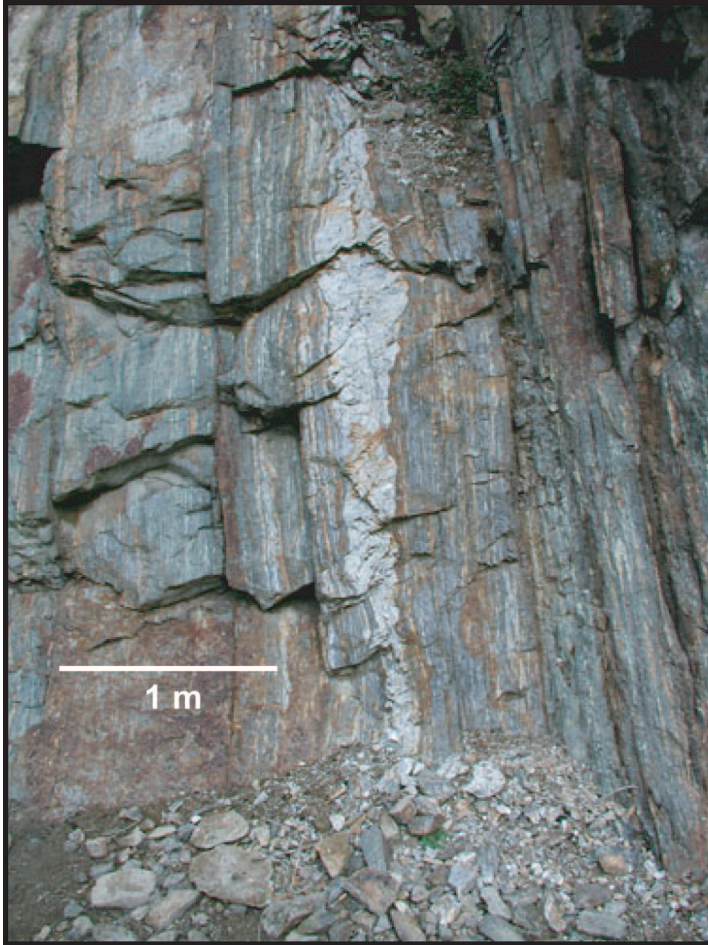
Fig. 3. Sample IG-2d – Deformed felsic melt pod (~50 cm across) within amphibolite section near Jiala.

zone, BT-19 is a syntectonic foliated muscovite-bearing granite east of the S/C mylonite zone, and BT-20 is a S/C mylonite with coarse augen. North of this traverse, BT-07 and NB-35-02 were collected near Dongjiu, from a garnet granite cutting Lhasa block gneisses and a granite cutting Lhasa metasediments, respectively.

Group C samples were collected from a large area west of the NB-GP massif. Sample NB-159-02 was collected from Lhasa block basement granitic gneiss near Loulan. Samples NB-120-02, BT19E, BT20E, BT-4-01 are spread out to the west of the NB-GP massif, in the general vicinity of Bayi and along the Nyang River. These, along with samples BT-36 and BT-37 (located considerably west, off the map, along the road to Lhasa from Bayi) most likely represent outcrops of Gangdese Arc granitoids.

Group D consists of two samples, BT-33 and BT-17-01 (2001 field season), collected from roughly north of the Namche Barwa massif, near Tungmai, in the area of the Jiali fault zone. Both represent granitic dikes intruding Lhasa Block metasediments of medium grade.

Group E samples were collected from northeast of Namche Barwa, in the vicinity of Bomi. Samples BM-02 and BM-03 represent Gangdese plutonic rock and were

Fig. 4. Sample BT-17-02 – Pegmatite dike cross-cutting basement gneisses, De'u Gungbu section, western margin of Gyala Peri massif.

collected from a granodiorite and a granite pegmatite dike, respectively, between Medog and Bomi. Samples BC-01, BC-02, and BC-03 are also Gangdese granitoids, collected along the main road to Qamdo and Chengdu, east of Bomi.

Mapping procedures.—The map (fig. 2) is based on the work of our Chengdu colleagues (Geng and others, 2002), modified and extended using observations made during our field work. Portions of original maps by Zhang and others (1992) and Burg and others (1997, 1998) for the eastern part of the syntaxis are also incorporated into figure 2.

Analytical techniques and considerations.—At the Stanford – U.S. Geological Survey Mass Analysis Center, we determined SHRIMP-RG (Sensitive High-Resolution Ion Microprobe – Reverse Geometry), U-Pb ages for all of the samples in this study. Zircons were separated using standard techniques of crushing, grinding, and heavy liquid and magnetic separation. Analyzed zircon fractions were primarily composed of clear, euhedral grains, and consistently exhibited one of two morphologies: elongate prisms
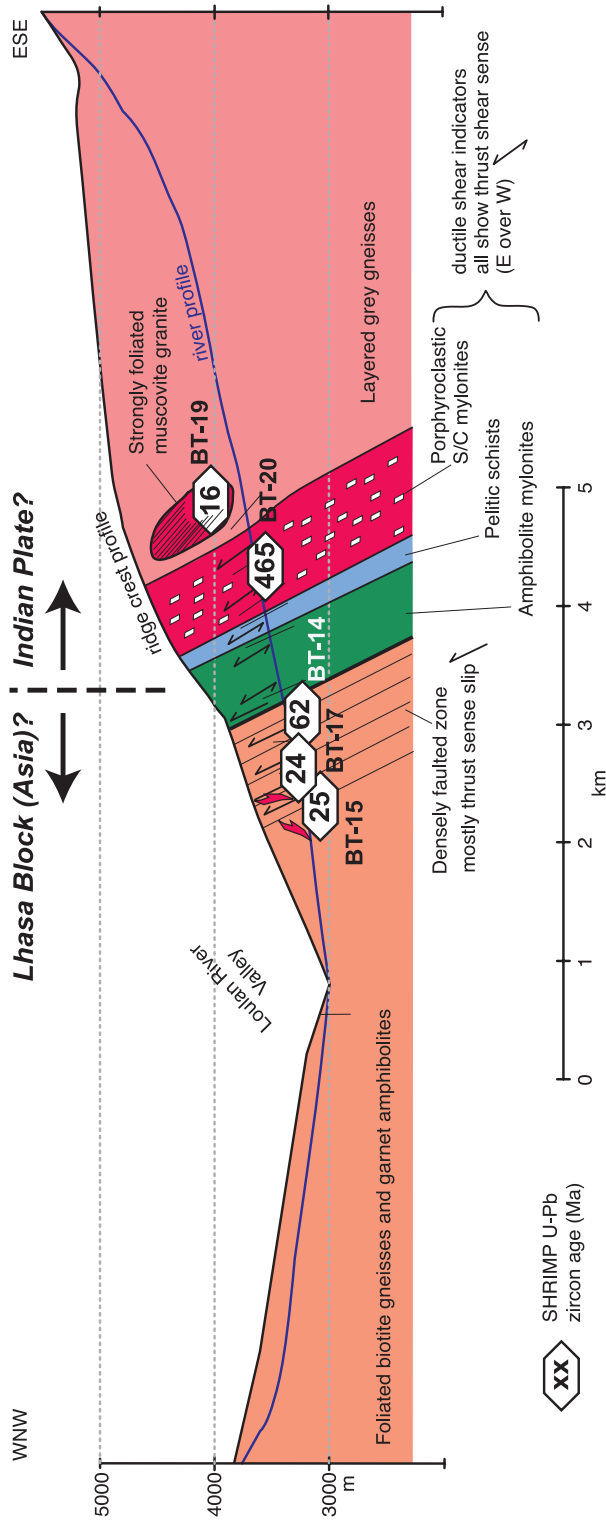
Fig. 5. Detailed cross-section (for location, see fig. 2) through the structural western margin of the Namche Barwa/Gyala Peri massif, on the western flank of the Gyala Peri massif (De'u Gungbu Valley). This section crosses the attenuated remnants of the Indus-Tsangpo suture. U-Pb zircon ages of samples are shown.
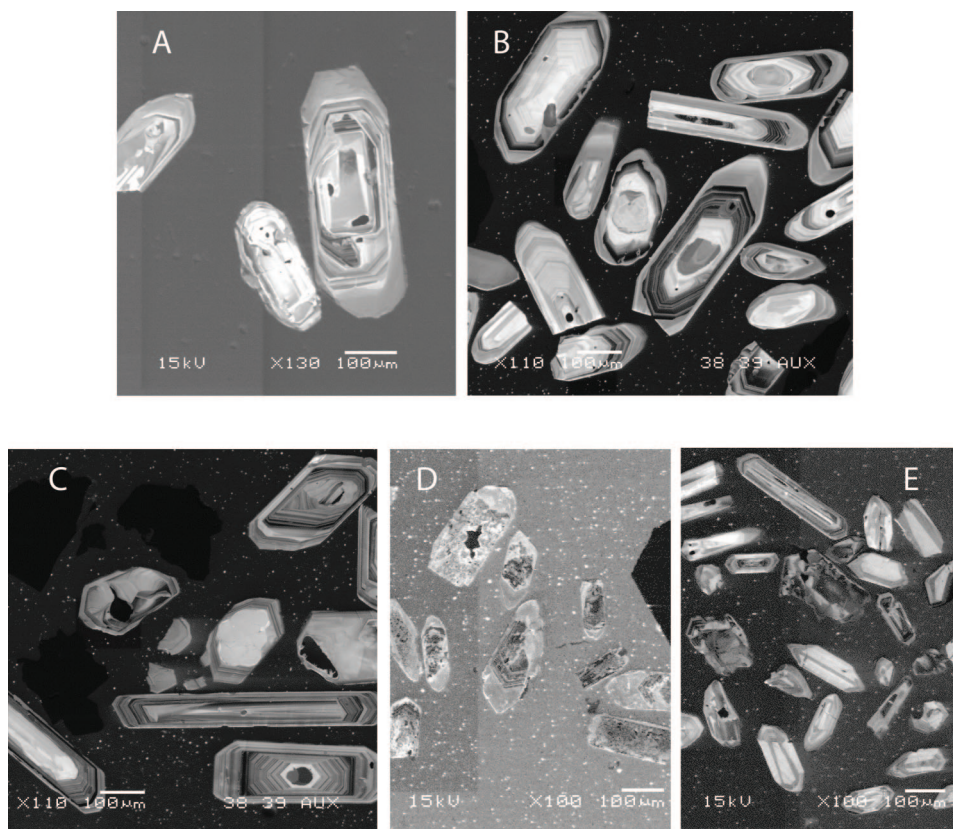
Fig. 6. Cathodoluminescence (CL) images of representative zircons from each sample group: (A) Namche Barwa (IG-16), (B) Northwest margin of NB-GP massif (BT-20), (C) Western Gangdese and related granitoids (NB-120), (D) North of Namche Barwa group (BT-33), and (E) Northeastern granites (BM-03), all showing strong zoning patterns.

or stubby prisms. Mineral coloring was honey yellow to light pink, with occasional inclusions of quartz, feldspar and biotite. Zircons from all sample groups were strongly zoned, and exhibited distinct cores with complicated overgrowths (fig. 6).

For each sample, separates were mounted in epoxy and polished to approximately half the mean grain thickness, then imaged with reflected light and cathodolumines-cence to illuminate internal zoning. The mounts were coated with gold for analysis and each sample was sputtered by using a primary beam of O$^-$ ions with a spot size of ~25 μm. Counts of Zr_2O, ^{204}Pb, background, ^{206}Pb, ^{207}Pb, ^{208}Pb, ^{238}U, ^{248}ThO, and ^{254}UO were measured from the secondary beam. Analytical and data reduction procedures followed those given in Williams (1998). For age standardization, concentrations of uranium and thorium from standard zircons SL13 and CZ3 were used. U/Pb ratios were determined through replicate analyses of standard zircons R33 (418 Ma) and AS57 (1099 Ma), and ages were based on the measured $^{206}Pb/^{238}U$ ratio calibrated to the $^{206}Pb/^{238}U$ ratio in the AS57 standard. The Pb/U ratio in the standard typically exhibited a calculated external spot-to-spot error of ~2.0% (2σ). All reported ages were determined using the data-reduction program Squid (Ludwig, 2001). Common Pb corrections were made using the two-stage average crustal Pb model of Stacey and Kramers (1975). Analyses yielding ages greater than 1000 Ma we corrected by using

measured ^{204}Pb, while younger ages were corrected using measured ^{207}Pb. Because our samples are primarily young (Mesozoic and younger), Tera-Wasserburg concordia plots are chosen as the most appropriate to display the analytical data (figs. 6-10).

Major and trace element analyses for 37 Namche Barwa area granites were obtained by employing conventional XRF (X-ray fluorescence) spectrometry at the Washington State University GeoAnalytical Laboratory. Of these, three samples (BT14-02, BT19E-02, NB02-159) included weathered pieces in those that were ground for analysis. All had good XRF totals, however, indicating that the amount of late-alteration hydrous material was not significant.

<div align="center">RESULTS</div>

Geochronology.—Our new U-Pb zircon ages place significant constraints on the timing of granitic melt generation in the Namche Barwa and adjacent regions. Analytical results (table 1) are shown on Tera-Wasserburg concordia plots in figures 7, 8, 9, 10 and 11. The majority of the ages are concordant, with some older, slightly discordant ages resulting from inheritance, as would be expected from crustally-derived partial melts.

As the scope of our study is focused primarily on correlations between age and location, we emphasize that the procedures used for age assignments are not statistically rigorous, such as a more precise age-focused study would be. The wide range of the determined ages allows us to make groupings based on spatial trends; these groups are distinct from each other, and do not overlap within a 95 percent confidence interval.

Final ages were assigned using the weighted mean 207-corrected ^{206}Pb/^{238}U age of a coherent group, discounting points that showed abnormally high U, high ^{204}Pb, or discordance. The assigned age for each sample is presented with its concordia diagram, along with the age error (2σ), number of analyses, and mean square of weighted deviates (MSWD) for the coherent group. Values of MSWD greater than one are indicative of errors beyond those strictly associated with analytical errors, and suggest geologic errors such as outliers or samples from more than one population are contributing to the overall age range. In samples where distinct core and rim populations were present, the final age always represents the rim age; core ages are plotted separately on a collective diagram, one per sampling group. Coherent age groups were extracted using a minimum 5 percent probability-of-fit, and a minimum 30 percent fraction of the total analyses to constitute a valid age group. In cases where no coherent age group was apparent, the age we present is an inferred age, chosen to be the most likely crystallization age for that sample based on the available data points. Because we are focusing primarily on the broad tectonic implications of these zircon ages, inferred ages are treated with equal consideration in our conclusions. The ages exhibit ranges that are geographically distinct, as can be seen in figure 2, and correspond to the five principle sampling groups previously outlined:

[A] For samples from within the Namche Barwa massif, five U-Pb SHRIMP ages fell between 2.9 and 9.7 Ma (fig. 7). Concordant core ages cluster around 400 to 500 Ma and 800 to 900 Ma. Details of each sample are as follows:

For sample IG-2d, 11 rim spots and 11 core spots were analyzed. Of the 11 rim ages, no coherent age group was apparent; several of these ages are a likely reflection of mixing between rim and core compositions; however, six ages fall between 13 and 15 Ma. The age presented (~14 Ma) is an average of these six ages, and is therefore approximate. In sample IG-4, 9 spots were analyzed; all were rim ages. The coherent age group was comprised of 4 spots, yielding a final (weighted mean) age of 3.0 Ma. In sample IG-6b, 10 rim spots and 7 core spots were analyzed. 9 rim ages comprised a coherent group, with a weighted mean of 9.7 Ma. In sample IG-15a, 10 rim spots and 4 core spots were analyzed. Both core and rim spots, however, yielded the same age

TABLE 1

Summary of U-Pb isotopic data for all granitoids, with samples grouped by geographic location as in figures 7-11: Namche Barwa, Northwest margin of NB-GP massif, western Gangdese/related, north of NB-GP massif, and Bomi region/Northeast of NB-GP massif.

Spot Name	core/ rim	comm 206* (%)	U (ppm)	Th (ppm)	232Th/ 238U	207corr 206Pb/238U Age** (Ma)	1σ err (Ma)	Total 238/206	err (%)	Total 207/206	err (%)	207r/ 235	err (%)	206r/ 238	err (%)	err corr
[A] Namche Barwa granites																
IG2D-1	rim	-0.34	4118	93	0.02	13.7	0.2	467.17	1.7	0.0540	6.5	0.02	6.4	.0021	1.7	.267
IG2D-2	rim	-0.38	2288	76	0.03	21.9	0.4	295.24	1.8	0.0428	7.6	0.02	7.3	.0034	1.8	.251
IG2D-3	rim	1.23	4105	82	0.02	13.9	0.3	461.56	1.8	0.0476	7.0	0.01	14.4	.0021	1.8	.127
IG2D-4	rim	-0.17	3677	52	0.01	30.6	0.4	209.23	1.2	0.0512	4.7	0.03	4.8	.0048	1.2	.259
IG2D-5	rim	-0.41	2846	102	0.04	16.4	0.4	396.07	2.2	0.0395	8.2	0.01	7.9	.0025	2.2	.277
IG2D-6	rim	-0.50	2902	92	0.03	14.7	0.3	441.08	2.1	0.0426	8.6	0.01	8.2	.0023	2.1	.256
IG2D-7	rim	-0.27	4262	124	0.03	17.1	0.3	375.70	1.6	0.0469	6.2	0.02	6.2	.0027	1.6	.252
IG2D-8	rim	1.91	1283	43	0.03	18.0	0.5	358.19	2.8	0.0429	11.4	0.01	43.8	.0027	3.0	.069
IG2D-9	core	0.03	2460	644	0.27	321.5	0.9	19.48	0.3	.0559	0.7	0.39	0.8	.0513	0.3	.345
IG2D-10	core	0.15	393	184	0.48	449.5	2.7	13.82	0.6	.0574	1.5	0.56	2.1	.0722	0.6	.284
IG2D-11	core	0.02	4813	509	0.11	461.7	0.8	13.45	0.2	.0573	0.4	0.59	0.5	.0743	0.2	.347
IG2D-12	core	0.13	1383	63	0.05	122.8	0.6	51.53	0.5	.0556	1.5	0.15	2.1	.0194	0.5	.234
IG2D-13	core	0.25	2345	1885	0.83	254.4	0.8	24.64	0.3	.0579	0.8	0.31	1.4	.0405	0.3	.215
IG2D-14	core	0.12	415	231	0.57	473.1	3.2	13.11	0.7	.0578	1.4	0.60	1.6	.0762	0.7	.429
IG2D-15	core	0.05	2184	321	0.15	331.2	1.1	18.89	0.3	.0563	0.7	0.41	0.8	.0529	0.3	.404
IG2D-16	core	-0.04	1430	171	0.12	365.0	1.2	17.12	0.3	.0561	0.9	0.45	1.0	.0584	0.3	.323
IG2D-17	core	0.15	1893	32	0.02	26.3	0.2	243.52	0.7	.0493	3.8	0.03	4.4	.0041	0.7	.170
IG2D-18	core	0.03	2640	208	0.08	277.2	1.2	22.63	0.4	.0566	1.3	0.34	1.4	.0442	0.4	.311
IG2D-19	core	0.10	531	320	0.62	468.4	2.1	13.23	0.4	.0587	1.2	0.60	1.5	.0755	0.4	.300
IG2D-20	rim	0.34	955	61	0.07	14.9	0.2	428.55	1.3	.0545	6.7	0.02	8.4	.0023	1.4	.163
IG2D-21	rim	0.00	3624	95	0.03	14.4	0.1	445.58	0.7	.0489	3.2	0.02	3.3	.0022	0.7	.218
IG2D-22	rim	3.49	3582	52	0.01	13.5	0.1	474.84	0.7	.0516	3.1	0.01	33.1	.0020	1.0	.032
IG4-1	rim	-1.48	4366	53	0.01	3.0	0.1	2133.42	3.6	0.0472	14.3	0.00	12.2	.0005	3.6	.299
IG4-2	rim	-1.27	6020	87	0.01	2.7	0.1	2391.50	4.0	0.0439	13.8	0.00	12.0	.0004	4.0	.336
IG4-3	rim	-0.36	13138	329	0.03	3.9	0.1	1660.00	1.8	0.0493	7.0	0.00	6.9	.0006	1.8	.255
IG4-4	rim	-0.39	18841	433	0.02	3.6	0.1	1747.49	1.9	0.0595	6.5	0.00	6.5	.0006	1.9	.286

TABLE 1
(continued)

Spot Name	core/rim	comm 206* (%)	U (ppm)	Th (ppm)	232Th/238U	207corr 206Pb/238U Age** (Ma)	1σ err (Ma)	Total 238/206	err (%)	Total 207/206	err (%)	207r/235	err (%)	206r/238	err (%)	err corr
IG4-5	rim	2.79	7860	111	0.01	2.8	0.1	2253.59	3.3	0.0654	11.5	0.00	40.7	.0004	3.8	.093
IG4-6	rim	0.97	4110	45	0.01	3.1	0.1	2066.44	2.0	0.0517	7.4	0.00	12.4	.0005	2.1	.168
IG4-7	rim	0.19	21265	543	0.03	3.6	0.0	1771.41	1.2	0.0533	2.9	0.00	3.6	.0006	1.2	.341
IG4-8	rim	-0.25	10818	275	0.03	3.8	0.1	1690.75	1.4	0.0476	3.9	0.00	4.0	.0006	1.4	.335
IG4-9	rim	1.21	4708	56	0.01	3.4	0.1	1871.63	1.9	0.0573	6.2	0.00	9.3	.0005	1.9	.200
IG6B-1	rim	-0.64	2709	79	0.03	9.5	0.2	668.02	2.4	0.0559	8.8	0.01	8.5	.0015	2.4	.278
IG6B-2	rim	-0.76	1656	43	0.03	13.4	0.4	470.54	2.6	0.0651	8.8	0.02	8.4	.0021	2.6	.305
IG6B-3	rim	-0.73	2433	70	0.03	9.8	0.3	644.23	2.5	0.0658	9.0	0.02	8.6	.0016	2.5	.295
IG6B-4	rim	-0.84	2395	70	0.03	9.3	0.3	687.78	2.7	0.0507	10.4	0.01	9.6	.0015	2.7	.282
IG6B-5	rim	-0.86	2131	61	0.03	9.7	0.3	665.36	2.7	0.0445	11.4	0.01	10.3	.0015	2.7	.265
IG6B-6	rim	-0.60	3152	93	0.03	9.9	0.2	651.99	2.3	0.0442	11.2	0.01	10.4	.0015	2.3	.221
IG6B-7	rim	-0.87	2432	69	0.03	10.0	0.3	623.46	2.8	0.0744	9.0	0.02	8.7	.0016	2.8	.317
IG6B-8	rim	-1.39	1364	30	0.02	9.8	0.4	659.39	3.5	0.0397	15.2	0.01	12.5	.0015	3.5	.280
IG6B-9	rim	1.64	2563	73	0.03	10.0	0.3	636.94	2.6	0.0526	10.0	0.01	27.1	.0015	2.9	.105
IG6B-10	core	-0.02	1239	660	0.55	854.6	3.7	7.07	0.4	0.0658	1.3	1.29	1.4	.1415	0.4	.323
IG6B-11	core	-0.02	1822	19	0.01	454.3	2.2	13.66	0.5	0.0582	1.6	0.59	1.7	.0732	0.5	.289
IG6B-12	core	-0.01	1566	773	0.51	859.4	4.0	7.03	0.5	0.0652	1.3	1.28	1.4	.1422	0.5	.344
IG6B-13	core	0.03	1435	522	0.38	775.6	3.3	7.84	0.4	0.0633	1.3	1.11	1.4	.1275	0.4	.306
IG6B-14	core	0.11	1021	439	0.44	841.7	4.2	7.20	0.5	0.0639	1.5	1.21	1.9	.1388	0.5	.269
IG6B-15	core	-0.02	1043	712	0.71	867.0	4.4	6.96	0.5	0.0660	1.5	1.31	1.6	.1436	0.5	.321
IG6B-16	core	-0.03	880	559	0.66	844.9	4.7	7.16	0.6	0.0649	1.7	1.25	1.8	.1397	0.6	.316
IG6B-17	rim	-1.28	1791	55	0.03	9.3	0.3	691.03	3.4	0.0464	13.5	0.01	11.6	.0015	3.4	.289
IG15A-1	rim	-2.00	1525	6	0.00	5.9	0.3	1097.81	4.2	0.0416	17.7	0.01	13.7	.0009	4.2	.304
IG15A-2	rim	-0.44	5765	28	0.01	6.6	0.2	983.55	2.3	0.0408	8.3	0.01	8.0	.0010	2.3	.284
IG15A-3	rim	-1.67	1702	5	0.00	6.3	0.2	1036.41	3.9	0.0411	16.1	0.01	12.9	.0010	3.9	.298
IG15A-4	rim	-1.86	1562	6	0.00	6.4	0.3	1011.37	4.1	0.0419	20.1	0.01	15.5	.0010	4.1	.262
IG15A-5	rim	-1.93	1529	6	0.00	6.3	0.3	1020.47	4.1	0.0450	17.2	0.01	13.7	.0010	4.1	.303
IG15A-6	rim	-1.47	1947	7	0.00	6.4	0.2	1015.94	3.6	0.0393	16.1	0.01	13.0	.0010	3.6	.274

TABLE 1
(continued)

Spot Name	core/rim	comm 206* (%)	U (ppm)	Th (ppm)	232Th/238U	207corr 206Pb/238U Age** (Ma)	1σ err (Ma)	Total 238/206	err (%)	Total 207/206	err (%)	207r/235	err (%)	206r/238	err (%)	err corr
IG15A-7	rim	4.13	1635	4	0.00	6.1	0.3	1054.88	4.0	0.0444	16.3			.0009	4.9	
IG15A-8	rim	-0.54	4832	25	0.01	6.6	0.1	974.28	2.2	0.0467	8.8	0.01	8.3	.0010	2.2	.262
IG15A-9	rim	0.60	7371	22	0.00	7.6	0.1	843.84	1.8	0.0484	6.2	0.01	10.5	.0012	1.8	.174
IG15A-10	rim	-1.26	1552	5	0.00	6.4	0.1	1006.03	2.3	0.0521	8.5	0.01	7.7	.0010	2.3	.294
IG15A-11	rim	0.01	1939	6	0.00	5.9	0.1	1085.15	2.1	0.0480	8.3	0.01	8.5	.0009	2.1	.250
IG15A-12	rim	-1.45	1670	6	0.00	6.0	0.2	1073.27	2.4	0.0427	11.5	0.01	9.7	.0009	2.4	.252
IG15A-13	rim	-1.41	1547	6	0.00	5.8	0.1	1100.02	2.4	0.0485	9.3	0.01	8.3	.0009	2.4	.292
IG15A-14	rim	-1.26	1471	5	0.00	6.4	0.2	1003.87	2.3	0.0509	10.7	0.01	9.4	.0010	2.3	.244
IG16-1	rim	-4.87	1182	7	0.01	3.9	0.3	1639.65	6.5	0.0590	23.4	0.01	16.0	.0006	6.5	.407
IG16-2	rim	-3.84	1262	9	0.01	4.2	0.3	1523.85	5.9	0.0464	24.3	0.01	16.2	.0007	5.9	.362
IG16-3	rim	8.15	6691	163	0.03	3.1	0.1	2063.73	3.5	0.0507	13.3			.0004	5.6	
IG16-4	rim	-3.75	1263	7	0.01	4.6	0.3	1385.28	5.8	0.0598	20.9	0.01	15.4	.0007	5.8	.377
IG16-5	core	0.11	1816	561	0.32	489.1	5.1	12.68	1.1	0.0574	0.8	0.61	1.5	.0788	1.1	.730
IG16-6	core	0.01	1632	980	0.62	487.4	5.1	12.74	1.1	0.0566	0.9	0.61	1.4	.0785	1.1	.766
IG16-7	core	0.00	1663	639	0.40	498.4	5.2	12.44	1.1	0.0571	0.9	0.63	1.4	.0804	1.1	.760
IG16-8	core	0.04	1782	714	0.41	487.6	5.1	12.73	1.1	0.0565	0.9	0.61	1.4	.0785	1.1	.754
IG16-9	rim	1.93	3120	40	0.01	3.2	0.1	1980.99	2.3	0.0614	8.0			.0005	3.6	
IG16-10	rim	0.76	1138	6	0.01	4.8	0.1	1340.25	3.0	0.0522	11.5	0.01	11.9	.0007	3.0	.252
IG16-11	rim	3.62	533	2	0.00	5.8	0.3	1068.70	4.1	0.0747	13.7			.0009	8.3	
IG16-12	rim	4.02	1062	6	0.01	4.0	0.2	1537.53	3.5	0.0778	11.6			.0006	6.7	
IG16-13	rim	3.09	1011	5	0.01	3.9	0.2	1612.43	5.2	0.0705	17.7	0.01	18.4	.0006	5.2	.280
IG18-1	rim	0.66	1743	38	0.02	144.4	1.6	43.74	1.1	0.0564	3.3	0.16	7.2	.0227	1.1	.161
IG18-2	rim	1.05	12461	521	0.04	2.8	0.1	2279.23	2.1	0.0545	8.0	0.00	15.9	.0004	2.2	.138
IG18-3	rim	1.33	15658	803	0.05	3.1	0.1	2051.82	1.8	0.0528	7.0	0.00	14.1	.0005	1.9	.135
IG16-4	rim	-3.75	1263	7	0.01	4.6	0.3	1385.28	5.8	0.0598	20.9	0.01	15.4	.0007	5.8	.377
IG16-5	core	0.11	1816	561	0.32	489.1	5.1	12.68	1.1	0.0574	0.8	0.61	1.5	.0788	1.1	.730
IG16-6	core	0.01	1632	980	0.62	487.4	5.1	12.74	1.1	0.0566	0.9	0.61	1.4	.0785	1.1	.766
IG16-7	core	0.00	1663	639	0.40	498.4	5.2	12.44	1.1	0.0571	0.9	0.63	1.4	.0804	1.1	.760

TABLE 1
(continued)

Spot Name	core/rim	comm 206*(%)	U (ppm)	Th (ppm)	232Th/238U	207corr 206Pb/238U Age** (Ma)	1σ err (Ma)	Total 238/206	err (%)	Total 207/206	err (%)	207r/235	err (%)	206r/238	err (%)	err corr
IG16-8	core	0.04	1782	714	0.41	487.6	5.1	12.73	1.1	0.0565	0.9	0.61	1.4	.0785	1.1	.754
IG16-9	rim	1.93	3120	40	0.01	3.2	0.1	1980.99	2.3	0.0614	8.0			.0005	3.6	
IG16-10	rim	0.76	1138	6	0.01	4.8	0.1	1340.25	3.0	0.0522	11.5	0.01	11.9	.0007	3.0	.252
IG16-11	rim	3.62	533	2	0.00	5.8	0.3	1068.70	4.1	0.0747	13.7			.0009	8.3	
IG16-12	rim	4.02	1062	6	0.01	4.0	0.2	1537.53	3.5	0.0778	11.6			.0006	6.7	
IG16-13	rim	3.09	1011	5	0.01	3.9	0.2	1612.43	5.2	0.0705	17.7	0.01	18.4	.0006	5.2	.280
IG18-1	rim	0.66	1743	38	0.02	144.4	1.6	43.74	1.1	0.0564	3.3	0.16	7.2	.0227	1.1	.161
IG18-2	rim	1.05	12461	521	0.04	2.8	0.1	2279.23	2.1	0.0545	8.0	0.00	15.9	.0004	2.2	.138
IG18-3	rim	1.33	15658	803	0.05	3.1	0.1	2051.82	1.8	0.0528	7.0	0.00	14.1	.0005	1.9	.135
IG18-4	rim	-0.43	15185	885	0.06	2.8	0.1	2253.70	1.9	0.0527	7.4	0.00	7.2	.0004	1.9	.271
IG18-5	rim	-0.02	1834	24	0.01	498.6	2.3	12.44	0.5	0.0568	1.5	0.63	1.6	.0804	0.5	.288
IG18-6	rim	-0.01	2663	36	0.01	510.7	2.0	12.14	0.4	0.0567	1.3	0.65	1.4	.0824	0.4	.283
IG18-7	rim	2.54	20928	1112	0.05	2.9	0.1	2213.17	2.9	0.0553	6.8	0.00	28.3	.0004	3.1	.108
IG18-8	rim	-0.02	2219	19	0.01	481.2	2.4	12.90	0.5	0.0566	1.5	0.61	1.5	.0775	0.5	.325
IG18-9	rim	-0.35	17201	511	0.03	3.0	0.1	2158.20	1.8	0.0506	6.9	0.00	6.8	.0005	1.8	.260
IG18-10	core	0.01	1887	20	0.01	501.0	5.2	12.36	1.1	0.0580	0.8	0.65	1.3	.0809	1.1	.797
IG18-11	core	0.00	2043	24	0.01	509.9	5.3	12.14	1.1	0.0579	0.8	0.66	1.3	.0824	1.1	.816
IG18-12	core	-0.01	1880	23	0.01	476.3	5.0	13.03	1.1	0.0572	0.9	0.61	1.4	.0768	1.1	.781
IG18-13	core	0.02	4772	116	0.03	517.2	9.1	12.02	1.8	0.0542	1.6	0.62	2.4	.0832	1.8	.747
IG18-14	core	0.01	3265	39	0.01	528.9	9.4	11.76	1.8	0.0533	4.1	0.62	4.5	.0850	1.8	.403
IG18-15	core	0.00	9605	72	0.01	582.7	10.2	10.64	1.8	0.0539	1.1	0.70	2.1	.0940	1.8	.843
IG18-16	core	0.02	4932	35	0.01	542.6	9.6	11.44	1.8	0.0547	1.0	0.66	2.1	.0874	1.8	.864
IG18-17	core	0.19	5377	47	0.01	529.0	9.3	11.77	1.8	0.0530	0.5	0.60	2.1	.0848	1.8	.866
IG18-18	core	-0.04	1801	17	0.01	505.8	9.1	12.35	1.8	0.0510	1.4	0.57	2.7	.0810	1.8	.679
IG18-19	core	0.00	5946	34	0.01	511.0	9.0	12.17	1.8	0.0543	0.9	0.61	2.0	.0822	1.8	.898
[B] NW margin of NB-GP massif																
BT07-02-1A	rim	1.36	294	45	0.16	57.6	1.2	110.81	2.1	0.0515	6.2	0.05	20.6	.0089	2.3	.110
BT07-02-2	rim	-0.63	392	45	0.12	39.7	0.8	161.23	2.0	0.0508	6.8	0.05	6.6	.0062	2.0	.302

TABLE 1
(continued)

Spot Name	core/ rim	comm 206 * (%)	U (ppm)	Th (ppm)	232Th/ 238U	207corr 206Pb/238U Age ** (Ma)	1σ err (Ma)	Total 238/206	err (%)	Total 207/206	err (%)	207r/ 235	err (%)	206r/ 238	err (%)	err corr
BT07-02-3	rim	-0.78	223	31	0.14	53.7	1.3	119.27	2.4	0.0497	8.6	0.07	8.1	.0084	2.4	.301
BT07-02-4	rim	-0.23	648	150	0.24	53.0	0.9	121.11	1.6	0.0466	4.4	0.06	4.5	.0083	1.6	.356
BT07-02-5	core	0.07	226	10	0.04	527.5	13.1	11.71	2.5	0.0590	2.3	0.69	3.5	.0853	2.5	.731
BT07-02-6	rim	-0.39	505	44	0.09	46.2	0.8	137.93	1.7	0.0542	5.2	0.06	5.2	.0073	1.7	.325
BT07-02-7	core	-0.06	166	94	0.58	929.3	15.3	6.36	1.6	0.0804	5.9	1.75	6.0	.1572	1.6	.262
BT07-02-8	rim	-0.90	280	47	0.17	38.1	0.9	167.73	2.3	0.0513	8.4	0.05	7.8	.0060	2.3	.292
BT07-02-9	rim	0.73	243	40	0.17	54.1	1.3	118.22	2.3	0.0506	12.1	0.05	16.8	.0084	2.3	.292
BT07-02-10	core	-0.22	338	75	0.23	197.4	5.0	31.97	2.5	0.0549	5.7	0.25	6.1	.0314	2.5	.410
BT07-02-11	rim	2.65	272	50	0.19	50.5	1.5	125.06	2.9	0.0613	13.2	0.04	24.9	.0078	2.9	.118
BT07-02-12	rim	2.47	257	28	0.11	41.2	1.0	155.12	2.3	0.0517	8.7	0.03	19.8	.0063	2.3	.119
NB35-02-1	rim	1.65	806	210	0.27	27.9	0.5	228.47	1.8	0.0542	5.8	0.02	18.2	.0043	2.0	.109
NB35-02-2	rim	-0.29	938	495	0.55	59.2	0.9	108.12	1.6	0.0486	4.7	0.07	4.8	.0093	1.6	.330
NB35-02-3	rim	-0.57	673	77	0.12	45.7	0.9	139.15	1.9	0.0553	6.3	0.06	6.1	.0072	1.9	.315
NB35-02-4	rim	-1.32	548	165	0.31	25.6	0.7	243.31	2.6	0.0718	8.3	0.05	7.8	.0042	2.6	.335
NB35-02-5	rim	-0.74	1190	546	0.47	24.1	0.5	267.27	2.1	0.0468	7.5	0.03	7.1	.0038	2.1	.293
NB35-02-6	rim	-10.04	49	27	0.56	22.6	1.8	239.32	6.6	0.1776	15.5	0.15	13.0	.0046	6.6	.511
NB35-02-7	rim	0.53	738	321	0.45	26.0	0.5	245.20	2.0	0.0540	7.1	0.03	10.0	.0041	2.1	.206
NB35-02-8	rim	1.62	496	187	0.39	26.3	0.7	244.25	2.6	0.0492	8.8	0.02	20.0	.0040	2.7	.136
NB35-02-9	rim	-3.77	167	108	0.67	22.7	1.0	276.55	4.2	0.0653	15.0	0.05	11.6	.0038	4.2	.363
NB35-02-10	core	0.02	353	196	0.57	1476.5	16.4	3.88	1.2	0.1000	1.0	3.54	1.6	.2574	1.2	.787
NB35-02-11	core	0.33	897	225	0.26	124.5	1.7	51.04	1.3	0.0522	3.1	0.13	4.3	.0195	1.4	.313
NB35-02-12	core	0.29	302	343	1.18	1537.6	17.3	3.70	1.3	0.0973	1.0	3.53	1.9	.2694	1.3	.663
NB35-02-13	core	-0.18	849	432	0.53	109.2	1.6	58.27	1.4	0.0518	3.6	0.13	3.8	.0172	1.4	.376
NB35-02-14	core	0.28	284	137	0.50	2368.4	25.0	2.25	1.3	0.1870	0.6	11.33	1.5	.4440	1.3	.854
NB35-02-15	core	3.07	355	131	0.38	23.3	0.8	267.20	3.2	0.0738	10.0	0.02	26.5	.0036	3.4	.128
NB35-02-16	core	0.30	2073	400	0.20	205.5	2.5	30.08	1.2	0.0711	1.5	0.31	2.3	.0331	1.2	.493
BT-14-02-1	rim	0.81	817	419	0.53	65.1	0.9	97.73	1.3	0.0544	3.7	0.07	8.5	.0101	1.4	.164
BT-14-02-2	rim	0.00	407	95	0.24	61.0	1.0	103.97	1.6	0.0565	4.5	0.07	4.8	.0096	1.6	.335

TABLE 1

(continued)

Spot Name	core/rim	comm 206* (%)	U (ppm)	Th (ppm)	232Th/238U	207corr 206Pb/238U Age** (Ma)	1σ err (Ma)	Total 238/206	err (%)	Total 207/206	err (%)	207r/235	err (%)	206r/238	err (%)	err corr
BT-14-02-3	rim	0.39	957	568	0.61	64.7	0.9	98.77	1.3	0.0502	3.0	0.07	4.5	.0101	1.3	.295
BT-14-02-4	rim	0.20	1198	363	0.31	61.5	0.8	104.16	1.3	0.0489	3.0	0.06	4.1	.0096	1.3	.322
BT-14-02-5	rim	2.54	502	49	0.10	44.1	0.7	144.65	1.7	0.0519	5.1	0.03	34.3	.0067	2.0	.059
BT-14-02-6	rim	1.31	900	353	0.41	63.3	0.9	99.98	1.4	0.0582	4.5	0.06	11.4	.0099	1.5	.134
BT-14-02-7	rim	0.71	597	118	0.20	58.2	0.9	109.64	1.5	0.0519	4.1	0.06	11.4	.0091	1.6	.140
BT-14-02-8	core	3.21	661	180	0.28	67.4	1.0	93.07	1.4	0.0647	3.2	0.05	24.3	.0104	1.7	.072
BT-14-02-9	core	0.87	400	135	0.35	62.0	1.2	102.03	1.8	0.0583	5.0	0.07	8.3	.0097	1.9	.225
BT15-02-1	rim	0.12	8347	229	0.03	25.3	0.3	254.34	1.3	0.0478	1.7	0.03	2.3	.0039	1.3	.589
BT15-02-2	rim	-0.04	16657	992	0.06	27.3	0.4	235.62	1.3	0.0472	1.2	0.03	1.8	.0042	1.3	.721
BT15-02-3	core	-3.10	123	70	0.59	82.0	1.9	77.75	2.3	0.0519	7.6	0.14	7.0	.0133	2.3	.335
BT15-02-4	rim	0.70	6550	279	0.04	26.5	0.4	242.94	1.3	0.0467	1.8	0.02	5.7	.0041	1.4	.240
BT15-02-5	rim	-0.27	2121	71	0.03	56.5	0.8	113.13	1.4	0.0498	3.1	0.06	3.3	.0089	1.4	.418
BT15-02-6	rim	-0.24	6077	147	0.03	24.0	0.3	267.14	1.4	0.0479	2.2	0.03	2.6	.0038	1.4	.528
BT15-02-7	rim	-0.99	547	131	0.25	67.0	1.1	95.37	1.7	0.0505	4.4	0.09	4.5	.0106	1.7	.374
BT15-02-8a	rim	-5.84	109	65	0.62	70.7	2.1	89.83	2.9	0.0551	10.1	0.16	8.5	.0118	3.0	.347
BT15-02-9	rim	-1.83	175	163	0.96	87.2	1.7	73.41	2.0	0.0483	6.0	0.12	5.9	.0139	2.0	.337
BT15-02-10	rim	0.13	12528	280	0.02	26.4	0.3	243.23	1.3	0.0475	1.4	0.03	2.0	.0041	1.3	.666
BT15-02-11	rim	1.23	4263	77	0.02	24.1	0.4	266.72	1.5	0.0488	2.9	0.02	9.1	.0037	1.5	.165
BT15-02-12	rim	0.65	6134	150	0.03	24.1	0.3	267.70	1.4	0.0449	2.6	0.02	5.7	.0037	1.4	.250
BT15-02-13	rim	0.86	9558	189	0.02	24.5	0.3	262.33	1.4	0.0483	1.9	0.02	5.1	.0038	1.4	.270
BT15-02-14	rim	0.25	15349	682	0.05	25.2	0.3	254.34	1.3	0.0483	1.5	0.03	2.6	.0039	1.3	.515
BT15-02-15	rim	0.10	9769	236	0.02	26.4	0.4	242.88	1.4	0.0489	1.7	0.03	2.3	.0041	1.4	.579
BT15-02-16	rim	0.06	9391	364	0.04	24.8	0.3	259.49	1.4	0.0448	1.9	0.02	2.4	.0039	1.4	.560
BT15-02-17	rim	0.14	11532	446	0.04	25.1	0.3	255.97	1.4	0.0470	1.8	0.02	2.6	.0039	1.4	.518
BT15-02-18	rim	0.06	8116	217	0.03	24.3	0.3	264.64	1.4	0.0480	2.1	0.02	2.6	.0038	1.4	.526
BT15-02-19	core	-2.19	233	76	0.33	42.9	1.3	149.49	3.1	0.0481	8.1	0.06	18.5	.0068	3.4	.184
BT15-02-20	core	1.04	1002	308	0.32	44.1	1.0	145.85	2.2	0.0459	4.1	0.03	10.8	.0068	2.2	.203
BT15-02-21	rim	1.18	4459	108	0.03	21.9	0.4	294.26	2.0	0.0436	2.8	0.02	10.9	.0034	2.0	.183
BT15-02-22	core	0.05	15005	686	0.05	24.2	0.4	266.80	1.8	0.0434	1.5	0.02	2.4	.0037	1.8	.762

Table 1
(continued)

Spot Name	core/ rim	comm 206 * (%)	U (ppm)	Th (ppm)	232Th/ 238U	207corr 206Pb/238U Age ** (Ma)	1σ err (Ma)	Total 238/206	err (%)	Total 207/206	err (%)	207r/ 235	err (%)	206r/ 238	err (%)	err corr
BT17-02-1	rim	-2.10	497	32	0.07	24.3	0.5	262.87	2.0	0.0532	6.2	0.04	6.0	.0039	2.0	.335
BT17-02-2	core	0.40	204	157	0.80	416.4	6.2	14.59	1.5	0.0763	2.0	0.69	2.9	.0682	1.5	.512
BT17-02-3	rim	0.81	357	29	0.08	24.0	0.6	267.36	2.3	0.0481	8.6	0.02	11.0	.0037	2.3	.214
BT17-02-4	core	-0.22	326	121	0.38	204.3	3.6	30.89	1.7	0.0546	2.7	0.25	3.8	.0324	1.8	.465
BT17-02-5	rim	-2.82	472	28	0.06	23.4	0.5	273.12	2.2	0.0508	7.4	0.04	6.8	.0038	2.2	.323
BT17-02-6	rim	-1.50	825	23	0.03	25.1	0.5	257.16	1.8	0.0450	5.8	0.03	5.6	.0039	1.8	.329
BT17-02-7	core	4.64	961	31	0.03	22.1	0.7	289.40	3.0	0.0500	9.6			.0033	4.0	
BT17-02-8	core	-0.08	578	80	0.14	1086.3	14.6	5.45	1.5	0.2522	1.5	6.40	2.1	.1835	1.5	.700
BT17-02-9	rim	4.95	676	38	0.06	24.2	0.5	263.68	2.1	0.0521	6.9			.0036	2.9	
BT17-02-10	rim	-1.00	1190	84	0.07	26.1	0.4	247.85	1.7	0.0430	6.1	0.03	5.7	.0041	1.7	.290
BT17-02-11	rim	1.17	1474	28	0.02	23.5	0.4	273.60	1.8	0.0479	4.7	0.02	8.8	.0036	1.8	.207
BT17-02-12	rim	-0.16	1216	12	0.01	88.6	1.3	71.78	1.5	0.0528	2.5	0.10	3.2	.0140	1.5	.453
BT17-02-13	rim	-1.91	757	38	0.05	24.1	0.5	267.21	1.9	0.0461	6.2	0.03	6.0	.0038	1.9	.324
BT17-02-14	rim	-0.74	838	185	0.23	59.8	1.0	107.28	1.7	0.0477	4.2	0.07	4.3	.0094	1.7	.386
BT17-02-15	core	-0.17	124	65	0.54	1421.6	20.6	4.06	1.6	0.0959	1.5	3.30	2.2	.2467	1.6	.735
BT17-02-16	rim	-2.81	620	35	0.06	22.4	0.6	286.70	2.4	0.0494	7.5	0.04	7.0	.0036	2.4	.350
BT17-02-17	core	1.71	533	155	0.30	21.8	0.7	292.71	3.0	0.0521	7.6			.0034	3.0	
BT17-02-18	core	-1.09	63	70	1.15	977.4	24.5	6.08	2.5	0.0752	7.2	1.92	10.8	.1662	2.7	.245
BT17-02-19	core	-5.79	199	98	0.51	21.3	1.0	302.94	4.4	0.0435	14.2			.0035	5.6	
BT17-02-20	core	-11.09	782	845	1.12	33.1	1.2	194.21	3.7	0.0471	11.2	0.10	48.4	.0057	9.0	.185
BT17-02-21	core	0.03	447	99	0.23	962.9	17.9	6.27	1.9	0.0636	3.5	1.39	4.0	.1595	1.9	.475
BT17-02-22	core	-0.16	534	78	0.15	417.5	8.8	14.17	2.0	0.0971	4.3	0.96	4.7	.0707	2.0	.418
BT17-02-23	core	-0.05	139	131	0.97	1580.9	31.0	3.60	2.2	0.1044	1.2	4.02	2.5	.2779	2.2	.872
BT17-02-24	core	-0.18	383	69	0.19	342.9	7.2	17.58	2.1	0.0853	1.7	0.68	3.2	.0570	2.1	.652
BT17-02-25	core	0.03	1159	42	0.04	212.7	4.0	29.80	1.9	0.0506	1.8	0.23	2.6	.0336	1.9	.721
BT19-02-1	rim	1.66	35	0	0.01	19.6	1.3	311.30	6.2	0.0896	18.9			.0032	6.3	
BT19-02-2	core	-9.06	29	1	0.04	89.3	3.3	71.41	3.7	0.0514	13.0	0.25	9.9	.0153	3.7	.375
BT19-02-3	rim	60.47	28	0	0.01	15.6	1.6	390.93	10.0	0.0901	26.6			.0010	24.8	

TABLE 1
(continued)

Spot Name	core/rim	comm 206* (%)	U (ppm)	Th (ppm)	232Th/238U	207corr 206Pb/238U Age** (Ma)	1σ err (Ma)	Total 238/206	err (%)	Total 207/206	err (%)	207r/235	err (%)	206r/238	err (%)	err corr
BT19-02-4	core	-15.25	19	1	0.06	105.6	5.8	61.10	5.5	0.0403	19.1	0.39	11.9	.0189	5.5	.465
BT19-02-5	core	-0.15	516	517	1.03	169.2	2.4	37.69	1.4	0.0476	2.9	0.18	3.6	.0266	1.4	.395
BT19-02-6	rim	298.94	10	0	0.01	19.1	2.6	315.51	12.6	0.0999	40.1	-1.09	76.7	-.0063	72.5	.945
BT19-02-7	rim	-72.83	32	0	0.00	14.0	1.3	449.33	9.0	0.0634	21.8	0.21	14.4	.0038	9.3	.643
BT19-02-8	core	-1.09	152	28	0.19	102.2	2.1	62.66	2.0	0.0469	6.5	0.12	11.9	.0161	2.2	.183
BT19-02-9	rim	8.96	67	1	0.02	16.0	0.9	395.08	5.6	0.0608	20.4			.0023	5.9	
BT19-02-10	rim	122.26	32	1	0.02	40.7	60.8	12.24	2.7	0.8006	2.8	-2.88	87.7	-.0182	70.8	.808
BT19-02-11	rim	97.05	39	0	0.01	16.5	1.3	383.06	7.8	0.0625	28.8			.0001	1161.6	
BT19-02-12	core	-2.70	81	6	0.08	114.8	2.6	55.88	2.3	0.0448	7.6	0.17	7.0	.0184	2.3	.327
BT19-02-13	rim	331.49	25	0	0.01	20.8	1.7	308.16	7.7	0.0516	32.6	-1.26	42.2	-.0075	39.0	.924
BT20-02-1	rim	0.97	745	160	0.22	523.6	7.4	11.80	1.4	0.0589	2.2	0.59	5.4	.0839	1.5	.272
BT20-02-2	rim	-0.02	947	889	0.97	479.4	6.2	12.94	1.3	0.0575	1.2	0.61	1.8	.0773	1.3	.747
BT20-02-3	rim	6.07	82	96	1.21	306.8	10.4	18.47	3.0	0.1333	5.7	0.60	29.7	.0508	4.2	.142
BT20-02-4	rim	0.23	2904	783	0.28	384.0	5.3	16.21	1.4	0.0585	1.4	0.48	2.6	.0616	1.4	.544
BT20-02-5	rim	3.71	1188	276	0.24	458.6	6.7	13.56	1.5	0.0564	2.2	0.25	28.2	.0710	1.6	.058
BT20-02-7	rim	0.00	1638	2189	1.38	490.8	6.5	12.63	1.4	0.0577	1.1	0.63	1.8	.0792	1.4	.764
BT20-02-8	rim	1.65	176	84	0.49	451.2	8.8	13.76	2.0	0.0582	4.0	0.44	18.3	.0715	2.2	.119
BT20-02-9	rim	-1.66	67	64	0.98	493.1	11.1	12.62	2.3	0.0546	5.6	0.75	5.6	.0806	2.3	.405
BT20-02-10	rim	-1.79	71	89	1.30	463.8	10.4	13.36	2.3	0.0590	5.6	0.77	5.6	.0762	2.3	.402
BT20-02-11	rim	-0.10	167	318	1.96	510.1	8.9	12.13	1.8	0.0584	3.5	0.67	3.9	.0825	1.8	.446
BT20-02-12	rim	-0.12	225	159	0.73	462.8	7.5	13.45	1.6	0.0555	3.0	0.58	3.5	.0744	1.6	.474
BT20-02-13	rim	-1.52	80	63	0.81	491.5	10.5	12.69	2.2	0.0524	5.4	0.71	5.4	.0800	2.2	.398
[C] Western Gangdese and related granitoids																
BT4-1	rim	-1.55	462	46	0.10	26.7	1.0	238.40	3.7	0.0554	13.6	0.04	11.9	.0043	3.7	.312
BT4-2	rim	-0.99	776	18	0.02	25.4	0.9	252.87	3.4	0.0464	11.8	0.03	10.7	.0040	3.4	.318
BT4-3	rim	5.87	447	61	0.14	26.8	1.1	239.91	3.9	0.0462	21.2			.0039	4.6	
BT4-4	rim	-1.38	556	68	0.13	26.1	0.9	245.08	3.5	0.0506	13.1	0.04	11.4	.0041	3.5	.308
BT4-5	rim	3.53	469	76	0.17	26.7	0.6	238.30	2.1	0.0569	7.9	0.02	26.8	.0040	2.2	.081

TABLE 1

(continued)

Spot Name	core/rim	comm 206* (%)	U (ppm)	Th (ppm)	232Th/238U	207corr 206Pb/238U Age** (Ma)	1σ err (Ma)	Total 238/206	err (%)	Total 207/206	err (%)	207r/235	err (%)	206r/238	err (%)	err corr
BT4-6	rim	2.66	221	65	0.30	26.1	0.8	240.17	2.9	0.0668	9.6	0.03	29.0	.0041	3.2	.110
BT4-7	rim	-1.09	458	65	0.15	25.6	0.6	249.62	2.2	0.0530	7.9	0.03	7.4	.0040	2.2	.302
BT4-8	rim	1.21	847	207	0.25	26.5	0.5	241.13	1.8	0.0510	5.8	0.02	10.3	.0041	1.8	.173
BT4-9	core	0.16	915	368	0.42	303.0	5.6	20.88	1.9	0.0486	1.6	0.31	2.7	.0478	1.9	.696
BT4-10	core	0.01	440	160	0.38	658.3	12.5	9.21	1.9	0.0694	3.7	1.04	4.2	.1086	1.9	.461
NB120-1	rim	-0.38	698	105	0.16	53.6	0.9	119.31	1.7	0.0504	7.1	0.06	6.9	.0084	1.7	.246
NB120-2	rim	0.96	484	92	0.20	49.3	1.0	130.25	2.1	0.0462	7.5	0.04	18.0	.0076	2.2	.121
NB120-3	rim	-0.14	1844	558	0.31	55.0	0.7	116.98	1.3	0.0451	3.4	0.05	3.6	.0086	1.3	.374
NB120-4	rim	0.23	1116	275	0.25	51.2	0.8	125.27	1.6	0.0476	4.8	0.05	6.0	.0080	1.6	.266
NB120-5	rim	-0.66	587	137	0.24	51.4	1.1	123.95	2.0	0.0529	6.8	0.07	6.6	.0081	2.0	.309
NB159-1	rim	0.34	1323	142	0.11	67.5	0.8	94.94	1.3	0.0483	2.6	0.07	3.8	.0105	1.3	.329
NB159-2	rim	-0.09	1345	291	0.22	66.3	0.8	96.63	1.3	0.0478	3.9	0.07	4.1	.0104	1.3	.308
NB159-3	rim	1.24	76	43	0.58	64.7	2.0	94.83	3.0	0.0827	8.8	0.10	13.9	.0104	3.1	.220
NB159-4	rim	0.29	1404	290	0.21	65.8	0.8	97.43	1.3	0.0473	3.2	0.06	5.2	.0102	1.3	.243
NB159-5	rim	0.92	471	250	0.55	63.3	1.0	100.76	1.6	0.0519	4.6	0.06	9.6	.0098	1.6	.169
NB159-6	rim	0.07	1436	90	0.07	63.4	0.8	100.97	1.3	0.0489	2.7	0.07	3.1	.0099	1.3	.407
NB159-7	rim	0.50	2813	479	0.18	68.7	0.8	93.29	1.2	0.0482	1.8	0.06	2.6	.0107	1.2	.447
BT19E-1	rim	-0.53	632	770	1.26	39.1	0.7	164.14	1.9	0.0487	6.3	0.04	6.1	.0061	1.9	.307
BT19E-2	rim	0.62	2970	1050	0.37	46.2	0.6	137.77	1.3	0.0541	2.7	0.05	6.3	.0072	1.3	.209
BT19E-3	rim	6.45	1299	389	0.31	43.0	0.7	140.34	1.4	0.0971	3.4	0.04	35.6	.0067	2.2	.062
BT19E-4	rim	0.27	3674	1152	0.32	42.5	0.5	150.60	1.3	0.0500	3.2	0.04	4.2	.0066	1.3	.308
BT19E-5	rim	-1.62	253	135	0.55	34.3	1.0	183.98	2.8	0.0615	9.7	0.06	8.7	.0055	2.9	.328
BT19E-6	rim	-0.29	1145	261	0.24	44.2	0.7	145.54	1.6	0.0455	4.9	0.05	5.0	.0069	1.6	.315
BT19E-7	rim	45.45	7460	1412	0.20	46.2	4.4	78.92	1.5	0.4004	1.8			.0069	6.4	
BT19E-8	core	81.32	312	192	0.64	97.2	82.7	8.27	1.4	0.7615	0.8			.0226	30.1	
BT19E-9	rim	75.78	174	114	0.68	44.0	29.1	23.04	2.0	0.7351	1.9			.0105	35.9	
BT19E-10	core	4.02	979	235	0.25	516.8	6.6	11.53	1.2	0.0880	2.9	0.64	11.4	.0833	1.3	.110
BT19E-11	rim	2.12	2768	1347	0.50	41.9	0.6	150.90	1.3	0.0595	2.8	0.04	14.2	.0065	1.5	.103

TABLE 1

(continued)

Spot Name	core/rim	comm 206 * (%)	U (ppm)	Th (ppm)	232Th/238U	207corr 206Pb/238U Age** (Ma)	1σ err (Ma)	Total 238/206	err (%)	Total 207/206	err (%)	207r/235	err (%)	206r/238	err (%)	err corr
BT20E-02-1	rim	-0.15	1399	395	0.29	49.8	0.7	128.77	1.4	0.0483	3.4	0.05	3.6	.0078	1.4	.377
BT20E-02-2	rim	0.45	1514	414	0.28	49.9	0.7	128.42	1.4	0.0482	3.3	0.05	5.6	.0078	1.4	.256
BT20E-02-3	rim	-0.21	1042	252	0.25	50.7	0.7	126.24	1.4	0.0492	4.0	0.06	4.1	.0079	1.4	.353
BT20E-02-4	rim	0.46	1676	216	0.13	48.3	0.7	132.39	1.5	0.0513	4.1	0.05	7.2	.0075	1.5	.211
BT20E-02-5	rim	1.29	1094	215	0.20	49.6	0.8	129.05	1.5	0.0491	4.4	0.04	11.9	.0076	1.6	.134
BT20E-02-6	rim	0.25	946	238	0.26	49.1	0.9	130.67	1.7	0.0486	4.7	0.05	5.9	.0076	1.7	.291
BT20E-02-7	rim	-3.75	94	64	0.71	44.9	2.0	136.46	4.3	0.0850	13.3	0.12	11.1	.0076	4.3	.384
BT36-02-1	rim	1.44	105	31	0.30	265.0	5.2	23.69	2.0	0.0563	5.5	0.26	10.5	.0416	2.0	.191
BT36-02-2	rim	-0.06	815	109	0.14	280.1	3.5	22.45	1.2	0.0543	2.1	0.34	2.4	.0446	1.2	.511
BT36-02-3	rim	-0.16	452	37	0.09	226.2	3.2	27.91	1.4	0.0535	3.3	0.27	3.5	.0359	1.4	.405
BT36-02-4	rim	0.25	1872	208	0.11	243.3	2.8	25.96	1.2	0.0523	1.7	0.27	2.7	.0384	1.2	.433
BT36-02-5	rim	2.20	126	22	0.18	246.3	5.0	25.62	2.0	0.0528	5.8	0.18	18.2	.0382	2.1	.116
BT36-02-6	rim	-0.29	167	71	0.44	260.4	4.5	24.18	1.7	0.0541	4.5	0.32	4.7	.0415	1.7	.366
BT37-02-1	rim	4.80	496	335	0.70	73.2	1.5	82.70	1.8	0.0925	4.4	0.09	30.1	.0115	2.6	.085
BT37-02-2	rim	1.28	752	871	1.20	63.0	1.0	100.78	1.6	0.0552	4.8	0.06	18.8	.0098	1.9	.100
BT37-02-3	rim	-0.42	419	228	0.56	70.6	1.3	89.51	1.8	0.0592	5.2	0.10	5.3	.0112	1.8	.341
BT37-02-4	rim	-0.51	408	423	1.07	67.6	1.3	94.66	1.9	0.0495	6.2	0.08	6.1	.0106	1.9	.308
BT37-02-5	rim	3.08	304	417	1.42	73.2	3.3	81.72	2.2	0.1017	29.6	0.13	49.1	.0119	3.5	.071
BT37-02-6	rim	-0.64	337	296	0.91	66.4	1.4	96.41	2.0	0.0491	6.9	0.08	6.7	.0104	2.0	.303
[D] Granites north of NB																
BT17-01-1	rim	-0.04	20444	764	0.04	23.4	0.2	275.03	0.7	0.0465	2.5	0.02	2.6	.0036	0.7	.277
BT17-01-2	rim	-0.05	20907	577	0.03	22.2	0.1	289.88	0.6	0.0462	2.5	0.02	2.6	.0035	0.6	.243
BT17-01-3	rim	0.43	5306	123	0.02	20.2	0.3	316.62	1.3	0.0527	4.8	0.02	7.1	.0031	1.3	.180
BT17-01-4	rim	-0.07	12974	242	0.02	21.8	0.2	294.79	0.8	0.0480	3.0	0.02	3.1	.0034	0.8	.248
BT17-01-5	rim	0.43	8866	215	0.03	21.5	0.2	300.01	0.9	0.0452	3.9	0.02	5.5	.0033	1.0	.175
BT17-01-6	rim	-0.01	27722	1349	0.05	23.1	0.2	278.34	1.0	0.0474	1.0	0.02	1.4	.0036	1.0	.727
BT17-01-7	rim	1.57	5669	155	0.03	19.2	0.2	332.50	1.2	0.0548	2.6	0.02		.0030	1.3	
BT17-01-8	rim	5.17	75	47	0.65	49.5	2.0	128.00	3.9	0.0583	14.3	0.02	10.4	.0074	4.7	.124

TABLE 1
(continued)

Spot Name	core/rim	comm 206* (%)	U (ppm)	Th (ppm)	232Th/238U	207corr 206Pb/238U Age** (Ma)	1σ err (Ma)	Total 238/206	err (%)	Total 207/206	err (%)	207r/235	err (%)	206r/238	err (%)	err corr
BT17-01-9	core	0.19	1120	368	0.34	103.5	1.4	61.13	1.4	0.0570	2.3	0.12	2.8	.0163	1.4	.490
BT17-01-10	rim	2.12	11308	147	0.01	21.8	0.3	290.32	1.1	0.0605	5.5	0.02	13.7	.0034	1.2	.087
BT17-01-11	rim	0.07	10256	253	0.03	19.9	0.2	322.94	1.1	0.0480	2.2	0.02	2.5	.0031	1.1	.439
BT17-01-12	rim	0.18	21461	541	0.03	22.6	0.2	284.53	1.0	0.0487	1.1	0.02	1.9	.0035	1.0	.535
BT17-01-13	rim	0.09	5064	94	0.02	19.0	0.2	338.73	1.2	0.0484	2.9	0.02	3.2	.0029	1.2	.375
BT17-01-14	core	-0.03	4004	38	0.01	20.2	0.4	319.34	2.0	0.0450	3.0	0.02	3.6	.0031	2.0	.554
BT17-01-15	core	0.45	17687	301	0.02	24.7	0.5	261.46	1.8	0.0450	1.3	0.02	3.5	.0038	1.8	.522
BT33-1	core	0.04	25142	310	0.01	30.3	0.3	212.28	1.1	0.0471	1.3	0.03	1.8	.0047	1.1	.621
BT33-2	rim	1.73	5030	17	0.00	20.2	0.3	315.76	1.3	0.0525	4.0	0.02	7.7	.0031	1.3	.165
BT33-3	rim	0.17	4767	16	0.00	20.1	0.3	320.29	1.3	0.0468	3.0	0.02	3.6	.0031	1.3	.357
BT33-4	rim	-0.11	4254	13	0.00	20.0	0.3	320.20	1.3	0.0526	3.1	0.02	3.3	.0031	1.3	.392
BT33-5	core	1.59	526	719	1.41	74.0	1.1	85.97	1.4	0.0536	3.7	0.06	16.2	.0114	1.6	.100
BT33-6	core	4.18	310	246	0.82	74.1	1.4	85.32	1.9	0.0585	5.4	0.04	61.0	.0112	2.4	.040
BT33-7	rim	0.12	20916	271	0.01	30.9	0.3	207.90	1.1	0.0481	1.0	0.03	1.7	.0048	1.1	.667
BT33-8	rim	0.73	3455	24	0.01	25.9	0.3	245.75	1.3	0.0546	2.4	0.03	6.1	.0040	1.3	.216
BT33-9	rim	0.55	4796	13	0.00	21.7	0.3	294.95	1.2	0.0508	2.3	0.02	5.1	.0034	1.2	.244
BT33-10	rim	0.83	4318	16	0.00	21.7	0.3	294.68	1.2	0.0508	2.5	0.02	7.4	.0034	1.3	.173
BT33-11	core	0.21	12767	229	0.02	33.8	0.4	189.97	1.1	0.0483	1.1	0.03	2.1	.0053	1.1	.540
[E] Northeast granites																
BC-01-02-1	rim	0.31	1883	1683	0.92	118.9	1.4	53.59	1.2	0.0502	1.6	0.12	3.1	.0186	1.2	.380
BC-01-02-2	rim	0.88	4051	2929	0.75	116.9	1.3	54.24	1.1	0.0546	1.1	0.12	4.8	.0183	1.2	.239
BC-01-02-3	rim	0.74	2726	2595	0.98	113.3	1.3	55.79	1.1	0.0570	2.2	0.12	4.4	.0178	1.2	.263
BC-01-02-4	rim	0.12	681	285	0.43	832.5	9.6	7.09	1.1	0.0853	0.8	1.64	1.5	.1410	1.1	.749
BC-01-02-5	rim	0.90	458	312	0.70	110.0	1.6	57.62	1.4	0.0548	3.4	0.11	10.1	.0172	1.5	.150
BC-01-02-6	rim	0.09	1924	848	0.46	115.8	1.3	55.02	1.2	0.0505	1.7	0.12	2.2	.0182	1.2	.541
BC-01-02-7	rim	0.78	392	276	0.73	111.2	1.7	57.31	1.6	0.0506	3.7	0.11	7.4	.0173	1.6	.215
BC-01-02-8	rim	0.02	2406	1859	0.80	119.8	1.4	53.32	1.1	0.0481	1.5	0.12	1.9	.0188	1.1	.609

TABLE 1
(continued)

Spot Name	core/rim	comm 206*(%)	U (ppm)	Th (ppm)	232Th/238U	207corr 206Pb/238U Age**(Ma)	1σ err (Ma)	Total 238/206	err (%)	Total 207/206	err (%)	207r/235	err (%)	206r/238	err (%)	err corr
BC02-02-1	rim	0.33	1753	1154	0.68	113.4	1.4	56.05	1.2	0.0529	1.8	0.12	3.1	.0178	1.2	.389
BC02-02-2	rim	4.23	890	391	0.45	107.0	1.5	57.41	1.3	0.0802	3.1	0.10	18.4	.0167	1.5	.081
BC02-02-3	rim	0.22	509	715	1.45	110.6	1.5	57.69	1.4	0.0496	3.3	0.11	4.0	.0173	1.4	.345
BC02-02-4	rim	0.21	2115	1354	0.66	119.0	1.4	53.60	1.1	0.0495	1.4	0.12	2.2	.0186	1.1	.516
BC02-02-5	rim	0.50	1042	657	0.65	116.5	1.4	54.72	1.2	0.0498	2.1	0.11	4.9	.0182	1.2	.252
BC02-02-6	rim	0.07	796	352	0.46	111.1	1.4	57.51	1.3	0.0482	2.6	0.11	3.0	.0174	1.3	.416
BC02-02-7	rim	0.35	10864	3300	0.31	134.4	1.5	47.35	1.1	0.0509	1.0	0.14	2.0	.0210	1.1	.542
BC03-02-1	rim	0.59	617	364	0.61	117.5	1.5	54.26	1.3	0.0496	2.8	0.11	5.7	.0183	1.3	.234
BC03-02-2	rim	0.12	472	253	0.55	114.8	1.7	55.37	1.5	0.0523	3.2	0.13	3.8	.0180	1.5	.384
BC03-02-3	rim	0.71	493	324	0.68	116.4	1.6	54.12	1.3	0.0598	2.7	0.14	4.4	.0183	1.3	.302
BC03-02-4	rim	-0.14	458	213	0.48	116.8	1.6	54.57	1.4	0.0498	3.2	0.13	3.5	.0183	1.4	.395
BC03-02-5	rim	1.09	683	446	0.67	113.0	1.5	56.11	1.3	0.0549	2.6	0.11	6.1	.0176	1.4	.225
BC03-02-6	rim	0.08	583	324	0.57	116.5	1.7	54.70	1.5	0.0507	4.0	0.13	4.4	.0183	1.5	.334
BM02-02-1	rim	3.07	135	83	0.64	113.2	2.2	54.72	1.9	0.0735	5.1	0.12	16.2	.0177	2.0	.125
BM02-02-2	rim	8.14	92	79	0.89	118.2	2.8	51.87	2.2	0.0812	7.1			.0177	3.9	
BM02-02-3	rim	0.17	1299	375	0.30	115.0	1.4	55.45	1.2	0.0496	1.9	0.12	2.4	.0180	1.2	.500
BM02-02-4	rim	0.36	156	112	0.74	119.3	2.5	53.76	2.1	0.0448	5.9	0.11	8.1	.0185	2.1	.255
BM02-02-5	rim	0.50	309	182	0.61	114.7	1.7	54.85	1.5	0.0611	5.2	0.14	7.5	.0181	1.5	.201
BM02-02-6	rim	-0.22	321	199	0.64	114.4	1.7	55.61	1.5	0.0515	4.0	0.13	4.1	.0180	1.5	.361
BM03-1	rim	5.86	300	341	1.17	61.1	1.2	103.68	1.9	0.0575	6.2	0.09		.0091	2.8	
BM03-2	rim	-0.56	287	198	0.71	62.7	1.2	100.64	1.9	0.0612	5.9	0.06	5.9	.0100	1.9	.331
BM03-3	rim	2.67	844	734	0.90	63.4	0.9	98.60	1.4	0.0683	3.3	0.06	20.0	.0099	1.8	.089
BM03-4	rim	1.77	586	423	0.75	64.6	1.0	98.12	1.5	0.0566	4.9	0.06	16.3	.0100	1.7	.104
BM03-5	rim	4.02	1719	4237	2.55	66.7	0.9	93.14	1.2	0.0730	2.0	0.06	21.0	.0103	1.5	.072
BM03-6	rim	0.36	1131	1977	1.81	65.6	0.9	97.37	1.3	0.0503	3.1	0.07	5.5	.0102	1.4	.246
BM03-7	core	0.02	2549	741	0.30	688.3	7.4	8.87	1.1	0.0631	0.5	0.98	1.2	.1127	1.1	.895
BM03-8	core	0.49	1289	1033	0.83	68.0	0.9	94.36	1.3	0.0467	2.9	0.06	7.2	.0105	1.3	.184

*from 207 correction

**common-Pb correction by assuming $^{206}Pb/^{238}U$–$^{207}Pb/^{235}U$ age-concordance; For ages > 1000 Ma, the value in this column is a 204-corrected age
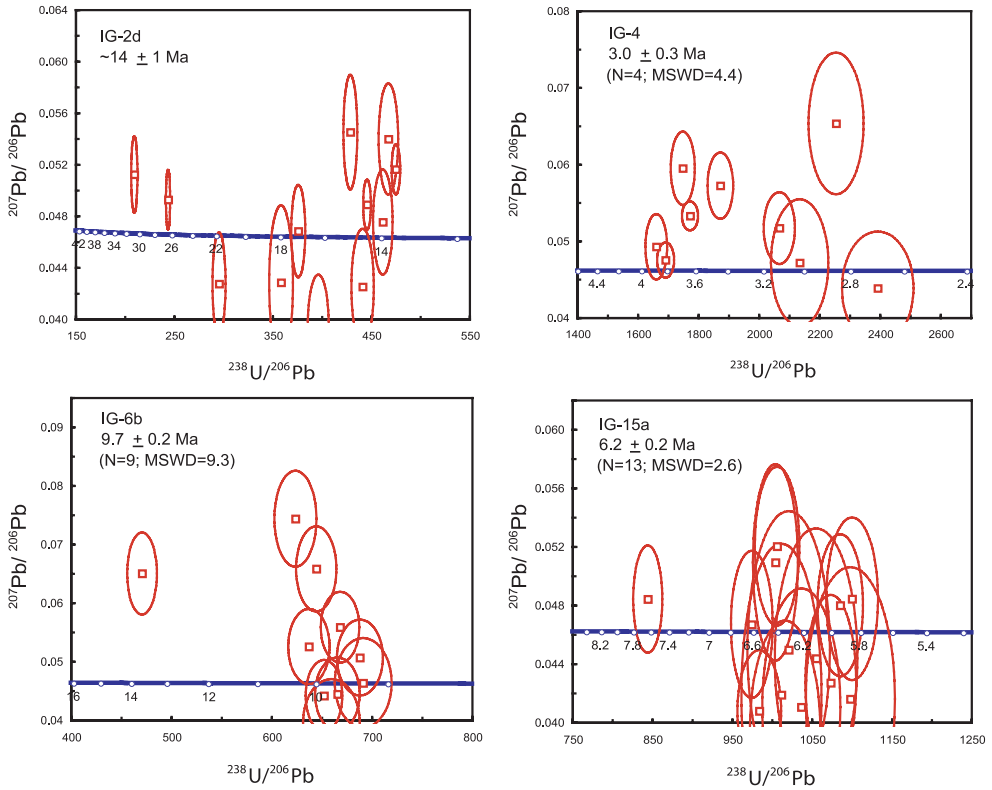
Fig. 7. Tera-Wasserburg concordia diagrams showing U-Pb SHRIMP ages for group A samples – from within the Namche Barwa massif. Error ellipses are shown at 2σ uncertainty. Older zircon core ages are shown, where applicable, for all samples on composite Concordia plot.

range (5 – 8 Ma). 13 analyses comprised a coherent age group, with a weighted mean of 6.2 Ma. In sample IG-16, 9 rim spots and 4 core spots were analyzed. Of the 9 rim ages, 6 comprised a coherent group with a weighted mean of 4.3 Ma. In sample IG-18, 9 rim spots and 10 core spots were analyzed. Some rim spots yielded ages as old as the cores, and many were discordant. Five rim ages, however, formed a coherent (young) age group with a weighted mean of 2.9 Ma.

[B] Along the northwestern margin of the NB-GP massif, the zircons are primarily Oligocene-Miocene in age (fig. 8), and were obtained from granitic bodies intruding both Lhasa block basement and Indian plate gneisses. Zircon core ages from this group show mostly Gangdese inheritance, except for sample BT-17, which exhibits protolith ages upwards of 1 Ga (Lhasa block material). Sample BT-20 also exhibited a Pan-African zircon rim age of 465 Ma.

Rim age populations for samples BT-14, BT-15, BT-17, BT-19, BT-20 and NB-35 all contained a coherent group, from which the final age (weighted mean) was extracted. BT-07 did not yield a coherent group, so the final age is approximate and equals the average (40 Ma) of the three youngest analyses, which clustered between 38 and 42 Ma.

[C] West of the NB-GP massif, our results fall primarily into the age range of ~40 to 70 Ma (fig. 9), with one 26 Ma age observed in sample BT-4, collected near Nyingchi. Another anomalous age (250 Ma – late Permian) was observed in sample BT-36, farther to the west, between Bayi and Lhasa (not shown on map; 29°58′23.0′′N
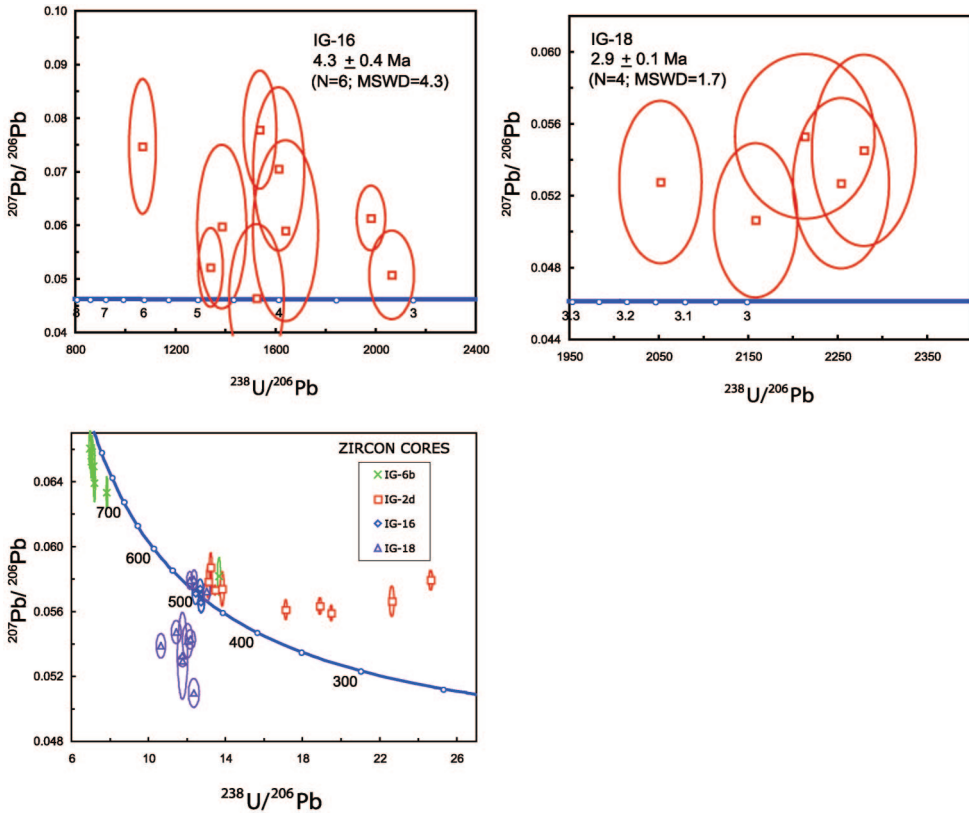
Fig. 7. (*continued*)

93°6′31.6″E). Sample BT-37 is also off the map (29°43′00.4″N 93°2′22.4″E), but yields a more-expected age of 72 Ma. Limited core ages for group C samples (660 Ma and 300 Ma for BT-4; 520 Ma and 97 Ma for BT-19E) suggest a Gondwanan protolith, plus some mixing between core and rim compositions.

All Group C samples had rim age populations that yielded coherent groups. Final ages, presented on figure 9, represent the weighted means of each of these groups.

[D] Two samples, BT-17-01 and BT-33, collected north of Namche Barwa along the Jiali fault zone yield 21 Ma ages (fig. 10). Core ages show evidence for a Gangdese protolith (74 Ma for BT-33; 100 Ma for BT-17-01). Rim ages for both samples exhibit a fair amount of scatter and did not possess a coherent age group; consequently these final ages are approximate. However, sample BT-17-01 shows a distinct cluster (N=11) of ages between 19 and 23 Ma, and BT-33 has a cluster (N= 5) between 20 and 22 Ma, allowing us to place reasonably good constraints on these approximations.

[E] Northeast of Namche Barwa, in the vicinity of Bomi, the zircon populations are as old as Mesozoic (113 - 118 Ma) in age (fig. 11), with one 63 Ma age. These samples (BM-02, BM-03, BC-01, BC-02, and BC-03) exhibited no distinct evidence of inheritance, and each age population yielded a coherent group. Final ages represent the weighted means of these coherent groups, and are expressed on figure 11.

Geochemistry.— All samples have bulk compositions within the range typical of peraluminous granites, consisting of quartz (20 - 35%), plagioclase (15 - 25%), K-feldspar (25 - 40%), and muscovite ± biotite (2 - 10%). Namche Barwa (Group A)
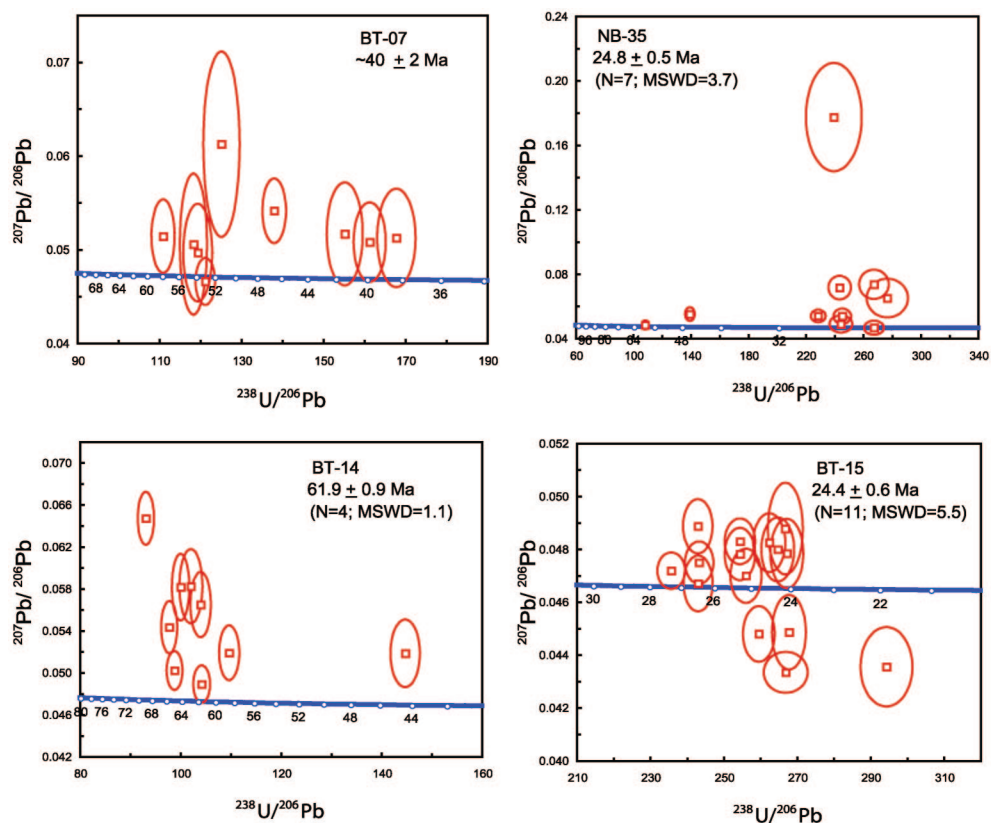
Fig. 8. Tera-Wasserburg concordia diagrams showing U-Pb SHRIMP ages for group B samples – from the northwest margin of the Namche Barwa-Gyala Peri massif. Error ellipses are shown at 2σ uncertainty. Older zircon core ages are shown, where applicable, for all samples on composite Concordia plot.

granitoids are characterized by high silica content (table 2), with 70 to 79 weight percent SiO_2, $Al_2O_3 > 12.0$ weight percent, and are metaluminous to slightly peraluminous (molar $Al_2O_3/(CaO + Na_2O + K_2O)$ ratios between 0.96 - 1.08). Rb/Sr ratios are high for this group (fig. 12), relative to granitoids outside the massif, with an average ratio of 3.8. Granitic bodies outside of the massif, north and west of Gyala Peri and northeast of Namche Barwa (Groups B, C, D, and E), are predominantly peraluminous and have notably lower Rb/Sr ratios.

Bulk geochemical abundances of the trace elements Rb, Y, and Nb indicate that the majority of the granites are calc-alkaline to alkaline, plotting in the field of volcanic arc granites (fig. 13) of Pearce and others (1984) and in the "post"-collision granite field of Pearce (1996).

<p style="text-align:center">INTERPRETATION</p>

Our study encompasses a series of granitic bodies that vary in their geochemistry and emplacement age, and occur within differing tectonic terranes. These granitoids are grouped as follows: [A] those intruded into Indian gneisses of Namche Barwa; [B] intruded into Lhasa block and Indian plate metasediments along the northwest margin of the NB-GP massif; [C] Gangdese Arc and related granitoids intruded into Lhasa block metasediments considerably west of the NB-GP massif; [D] intruded into
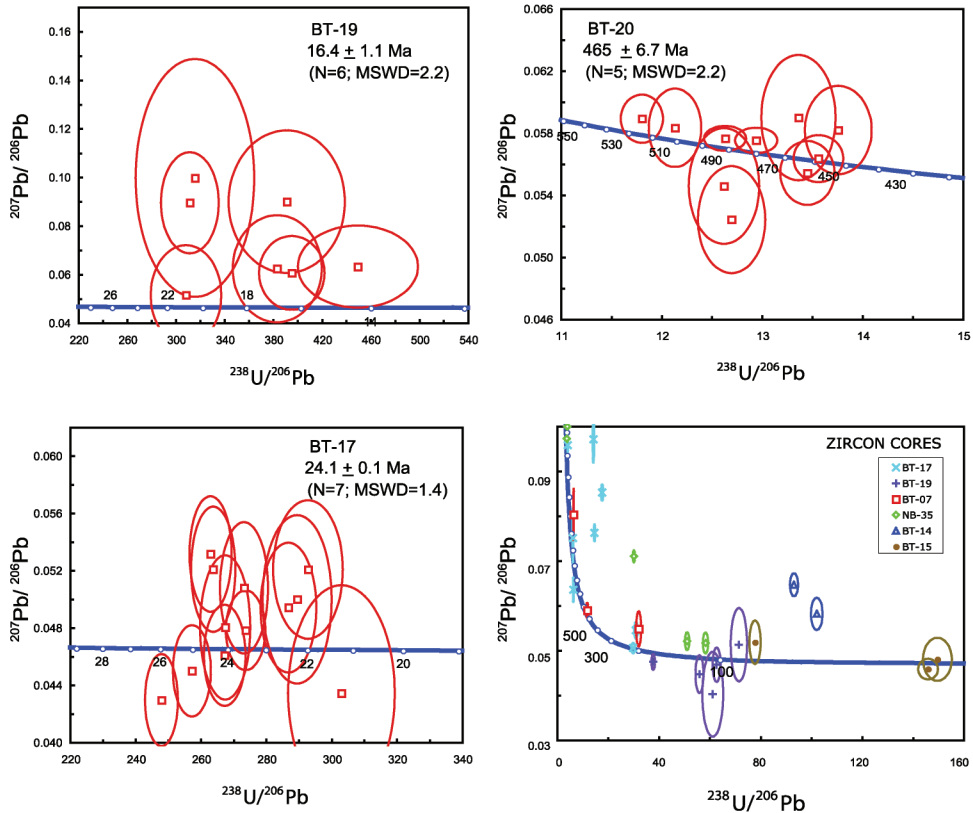
Fig. 8. (*continued*)

Lhasa block gneisses and metasediments north of Namche Barwa, near the Jiali fault zone; and [E] Gangdese Arc granitoids intruded into Lhasa block gneisses and metasediments northeast of Namche Barwa. We interpret the emplacement of these five groups of granites to be related to a series of different tectonic events impacting southeastern Tibet during Mesozoic-Cenozoic time.

Geochronology.—Our results for granite emplacement ages from Group A samples (Namche Barwa massif) are in good agreement with those reported by both Burg and others (1997) and Ding and others (2001), and support the evidence for exceptionally recent granitic activity near the massif core. Previously determined ages (Burg and others, 1997; Ding and others, 2001) combined with the results of this study define a distinct group of young crystallization ages for Namche Barwa massif samples. Also apparent is a well-defined population of 400 to 500 Ma core ages, possibly reflecting an event of regional high-grade metamorphism and melting during early Paleozoic time. Such evidence lends additional support to the concept of an early Paleozoic thrust event within Greater Himalayan rocks, as suggested by the studies of DeCelles and others (2000) and Gehrels and others (2003), and could indicate that Namche Barwa massif rocks may have undergone a similar history.

Group B samples (northwest margin of the NB-GP massif) contain protolith ages that help to delineate the ITSZ west of Gyala Peri. Within this transect across the suture (fig. 5), younger granitoids are present with ages of 24 Ma, but core ages indicate
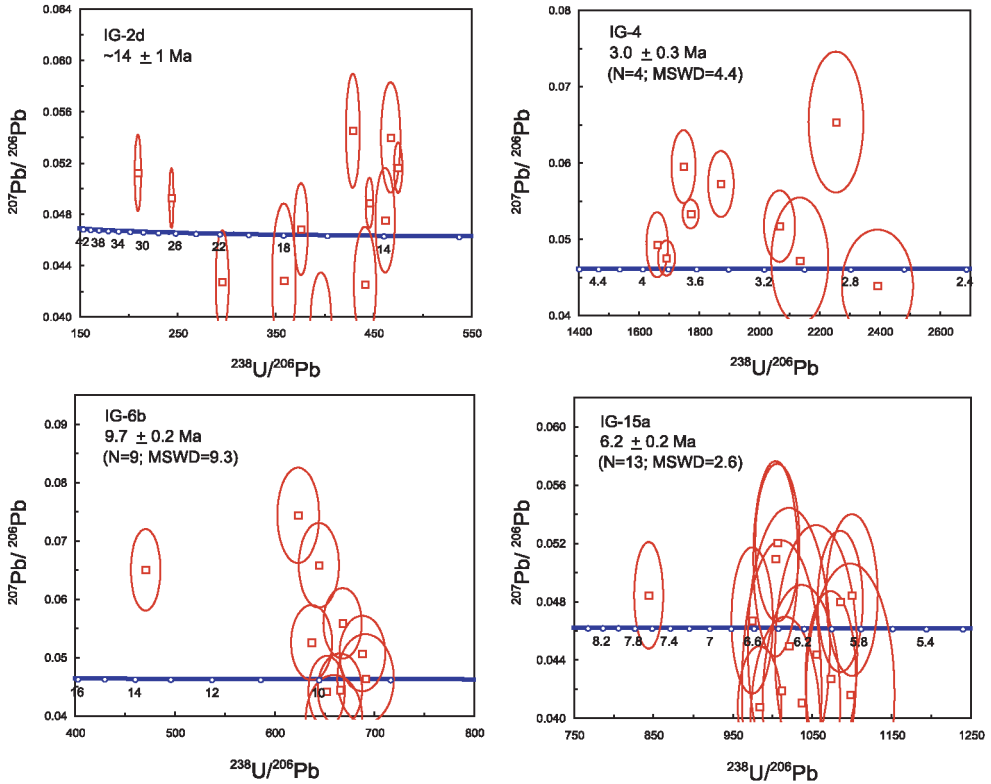
Fig. 9. Tera-Wasserburg concordia diagrams showing U-Pb SHRIMP ages from group C samples – from western Gangdese and Gandgese-related samples. Error ellipses are shown at 2σ uncertainty. Older zircon core ages are shown, where applicable, for all samples on composite Concordia plot.

inherited signatures that jump sharply from Gangdese in the west (67 Ma for BT-14 and 82 Ma for BT-15) to Indian in the east ("Pan-African" age of 465 for BT-20).

Group C samples (west of Namche Barwa) exhibit a cluster of crystallization ages between 40 to 70 Ma, corresponding to Gangdese plutonism. Sample BT-36, however, yielded a crystallization age of 250 Ma, which is not a surprising result, considering Permian rift-related rocks have been documented in the southern Lhasa block (Dewey and others, 1988).

Group E samples (northeast of Namche Barwa) contain numerous ages that correspond to Gangdese plutonism. Two isolated 21 Ma ages (Group D) in the north, however, are too young to be related to this subduction-related magmatism. Considering the widespread documentation of magmatism along the Red River shear zone (for example, Leloup and Kienast, 1993; Zhang and Schärer, 1999), and partial melts with emplacement ages around 22 to 23 Ma, the 21 Ma granitoids may be analogous to these melts. However, because these and similar other dikes consistently cut the ductile foliation of the gneisses in and near the Jiali fault zone, these granitic bodies are not likely to be a product of the shearing related to movement within this zone. Instead, we suggest they are perhaps related to the Gangdese Thrust event, which is of this age (~27 - 18 Ma) and involved underthrusting of part of the Gangdese belt (Copeland and others, 1995; Yin and others, 1999; Harrison and others, 2000). The role of the Gangdese Thrust, however, is controversial (that is, Aitchison and others, 2003).
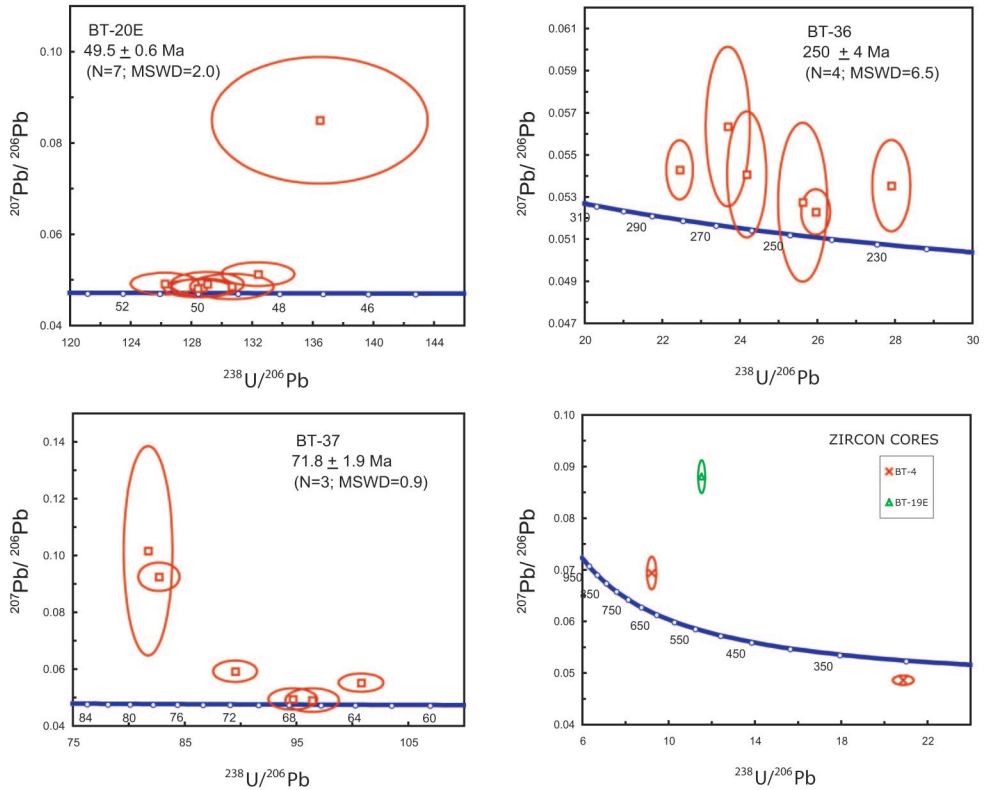
Fig. 9. (*continued*)

Therefore, an alternative means of production for the ~21 Ma granites might be slab break-off or slab detachment. Both of these mechanisms are suggested to have occurred at ~25 Ma (Kosarev and others, 1999; Miller and others, 1999; Chemenda and others, 2000; Yin and Harrison, 2000; Maheo and others, 2002; Kohn and Parkinson, 2002; Tilman and others, 2003).

Overall, in addition to the expected evidence for activity related to the Gangdese Arc, there is clear evidence in our results for a widespread partial-melting event around 20 to 25 Ma, and a much-younger (3 - 10 Ma) melting episode observed only at Namche Barwa. Geochemical data from the granites provides some insight as to the nature of these two young events.

Geochemistry.—Granitoids from within Namche Barwa exhibit a high Rb/Sr ratio (greater than 1.4), with notably greater frequency than outside the massif (fig. 12). It has been shown (Harris and others, 1993; Whittington and others, 1999) that trace element abundances in granitic rocks can provide information regarding the conditions prevalent during melting. A study by Harris and Inger (1992) predicted the consequences of fluid-present and fluid-absent melting for the composition of pelite-derived granites, in terms of the trace elements Rb, Sr and Ba. For granite systems, only these three elements reside predominantly in the major reactants and products of melting reactions (micas and feldspars). Concentration ratios (C_l/C_o) in the liquid relative to the source are calculated from appropriate partition coefficients (K_D) for granitic melts, using a range of values from Nash and Crecraft (1985), Blundy and
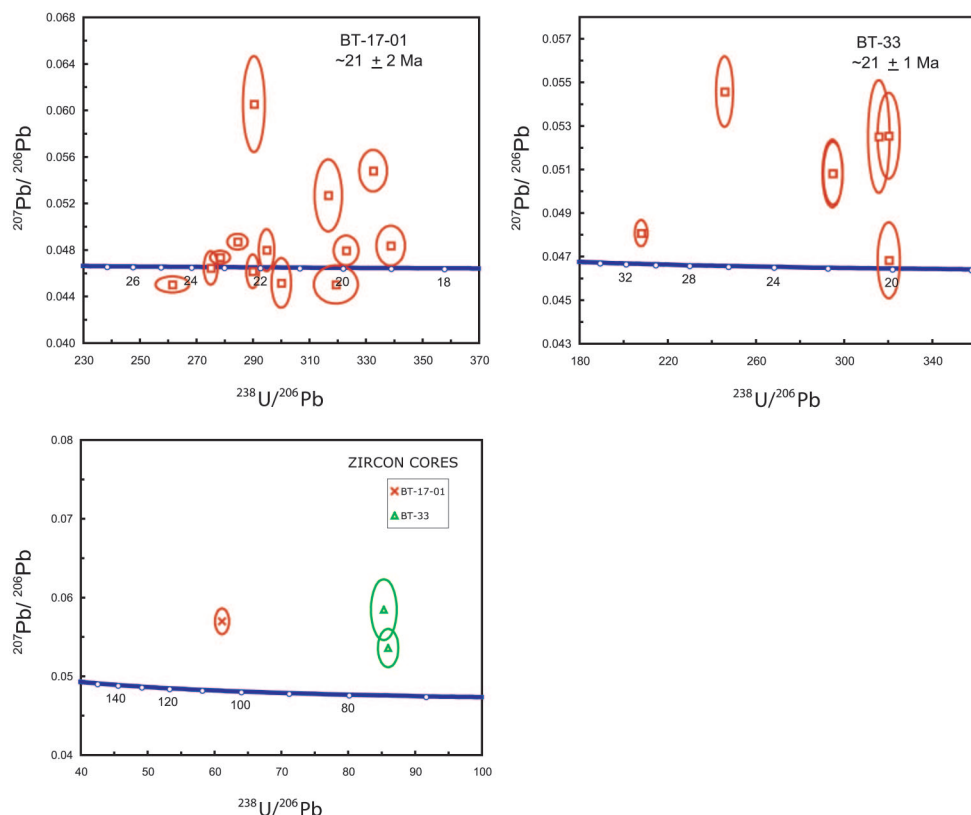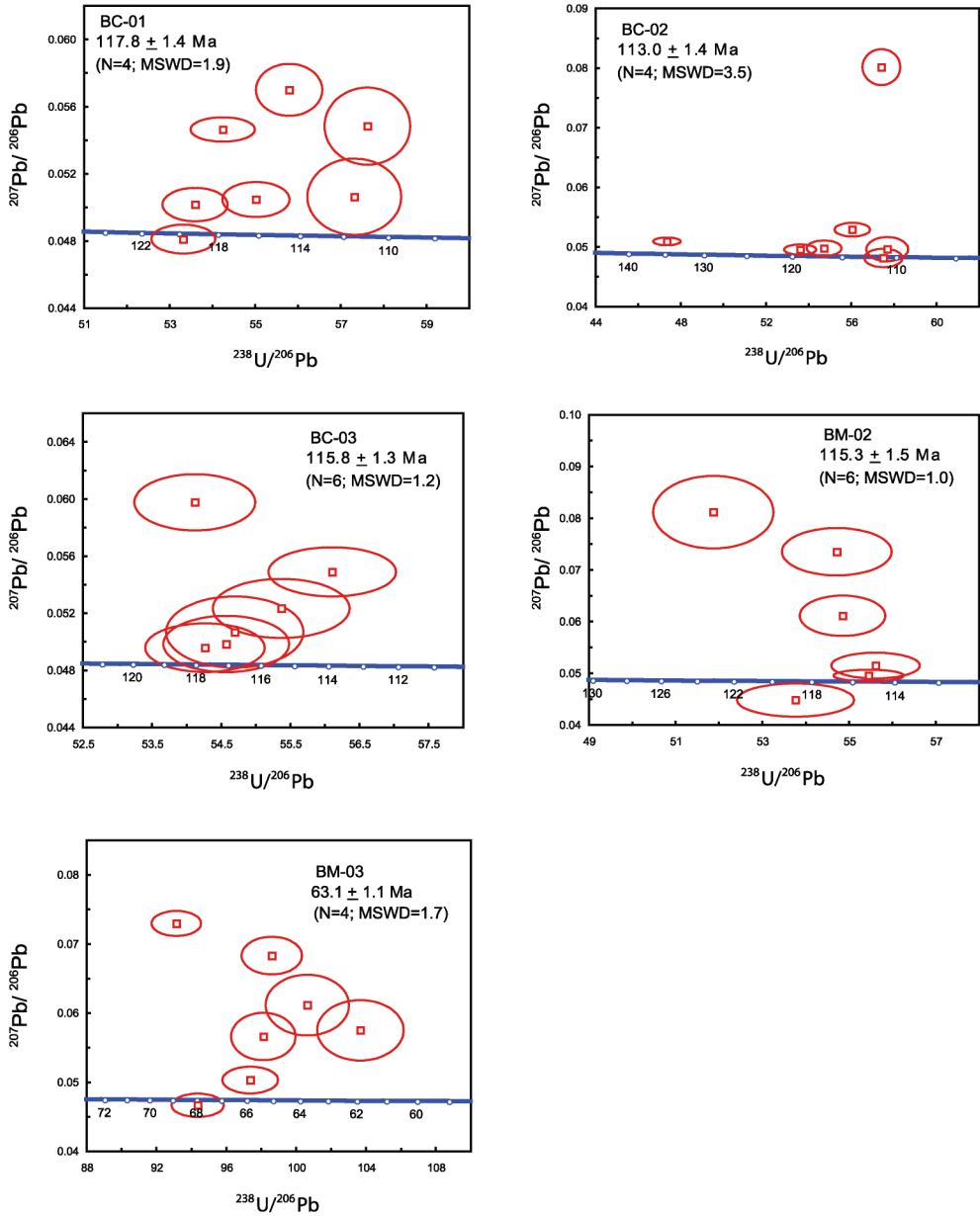
Fig. 10. Tera-Wasserburg concordia diagrams showing U-Pb SHRIMP ages for group D samples – from north of the Namche Barwa-Gyala Peri massif. Error ellipses are shown at 2σ uncertainty. Older zircon core ages are shown, where applicable, for all samples on composite Concordia plot.

Wood (1991), and Harris and others (1993). Simple melts have well-defined C_l/C_o ratios for Rb, Sr and Ba, whether controlled by mineral fractionation or by partial melting (Whittington and others, 1999). Fluid-present melting results in low Rb/Sr ratios and depleted Ba relative to the source, whereas fluid-absent melting results in high Rb/Sr ratios and enrichment of Ba. Geochemical modeling of Rb and Sr during anatexis suggests that fluid-absent breakdown of muscovite would produce melts with Rb/Sr ratios >1.5 (Harris and Inger, 1992).

The majority of the Namche Barwa samples (group A) exhibit relatively high Rb/Sr ratios (>1.4) suggesting that a fluid-absent melting (decompression) regime dominates near the massif core. Meanwhile, granitoids from groups B, C, D and E exhibit Rb/Sr ratios consistently below 1.5 (table 2) and imply fluid-present melting in these surrounding regions.

A particularly interesting result is that the Namche Barwa granites with the youngest U-Pb zircon ages (3.0 Ma and 2.9 Ma, samples IG-4 and IG-18) exhibit a low Rb/Sr ratio, implying a fluid-present melting history. This result has implications for both the rate of melt emplacement and the degree of meteoric water circulation at Namche Barwa. Moreover, the presence of both fluid-absent and fluid-present melts is significant, as it resembles conditions at Nanga Parbat in the western Himalayan syntaxis. At Namche Barwa, the predominance of fluid-absent "decompression" melts

Fig. 11. Tera-Wasserburg concordia diagrams showing U-Pb SHRIMP ages for group E samples – from the area of Bomi, northeast of the Namche Barwa-Gyala Peri massif. Error ellipses are shown at 2σ uncertainty.

could be a reflection of numerous varying parameters: (1) the sample locality bias—it is considerably more difficult to collect samples from the core of the massif as opposed to the lower-elevation flanks; (2) the uplift rate—if it were sufficiently rapid everywhere, only rarely could assemblages be preserved that were allowed to cool above the wet pelite solidus; (3) the degree of meteoric fluid circulation—how deep and how

TABLE 2

Major and trace-element geochemistry of southeastern Tibet granitoids, grouped by geographical location as in table 1 and figures 7-11.

| Sample | Namche Barwa massif granitoids | | | | | | NW margin of NB-GP massif | | | | | | |
| | IG-2d | IG-4 | IG-6b | IG-15a | IG-16 | IG-18 | BT-14 | BT-15 | BT-17 | BT-19 | BT-20 | NB02-35 | BT-7 |
Description	felsic melt pod	peg.	felsic dikelet	granitic sweat	granitic sweat	granite	granitic gneiss	granite peg.	granite dike	musc. granite	S/C mylonite	granite	gar. granite
(wt. %)													
SiO_2	75.35	79.00	77.58	70.32	71.98	72.95	73.36	72.84	69.95	72.24	69.95	63.78	71.96
Al_2O_3	12.04	12.35	12.08	17.62	13.84	15.28	14.30	16.60	16.42	16.98	14.25	18.75	14.88
TiO_2	0.186	0.046	0.198	0.104	0.391	0.030	0.267	0.026	0.328	0.053	0.545	0.608	0.327
FeO	2.27	0.30	0.76	1.34	2.31	0.28	2.38	0.25	1.69	0.54	3.50	3.65	2.18
MnO	0.041	0.004	0.014	0.035	0.036	0.005	0.026	0.005	0.021	0.028	0.067	0.053	0.051
CaO	1.12	2.94	1.79	5.54	2.34	1.86	3.23	3.73	2.21	2.48	1.80	4.42	2.86
MgO	0.31	0.20	0.40	0.67	0.76	0.20	0.57	0.13	0.67	0.20	0.67	1.24	0.64
K_2O	5.45	1.15	3.81	0.62	5.19	5.86	1.03	0.31	4.28	0.96	5.50	1.87	3.09
Na_2O	2.57	3.44	2.77	3.91	2.76	3.04	3.94	5.60	3.76	6.34	2.79	4.56	3.32
P_2O_5	0.016	0.007	0.031	0.029	0.091	0.011	0.071	0.011	0.063	0.044	0.158	0.231	0.061
Total	99.35	99.44	99.44	100.18	99.70	99.52	99.18	99.50	99.39	99.87	99.23	99.17	99.37
(ppm)													
Ni	11	5	18	3	4	1	3	5	4	6	8	5	6
Cr	0	1	0	3	3	0	0	0	0	0	2	0	3
Sc	3	2	1	3	6	3	9	6	7	1	17	14	6
V	18	0	17	31	33	0	27	6	20	14	25	55	33
Ba	607	132	300	79	718	1673	245	128	1154	256	1107	483	657
Rb	259	56	146	20	242	170	28	9	112	9	216	85	78
Sr	43	127	70	323	171	197	442	486	440	669	89	878	324
Zr	272	36	289	61	181	45	129	21	106	52	409	244	143
Y	107	1	87	8	28	5	5	7	7	2	79	14	15
Nb	22.7	1.8	16.3	2.4	14.4	1.8	4.9	2.9	12.3	1.7	30.6	7.5	8.5
Ga	19	14	18	15	17	12	17	16	17	14	23	22	15
Cu	10	0	2	16	4	4	2	8	0	17	2	6	1
Zn	36	5	5	14	25	3	34	7	29	21	55	80	38
Pb	10	8	2	13	16	29	10	31	51	3	21	16	21
La	95	0	119	10	42	0	62	4	108	0	145	54	21
Ce	142	11	233	15	82	0	99	16	210	0	251	101	60
Th	50	0	95	2	68	1	16	0	42	1	47	10	10
Y + Nb	130	3	103	10	42	7	10	10	19	4	110	22	24
Rb/Sr	6.023	0.441	2.086	0.062	1.415	0.863	0.063	0.019	0.255	0.013	2.427	0.097	0.241
A/CNK	0.990	1.008	1.012	1.026	0.960	1.038	1.062	1.017	1.107	1.063	1.031	1.068	1.062

TABLE 2
(continued)

	Western Gangdese and related granites						Granitoids north of NB			Northeastern granites			
Sample	BT-4-01	BT-20E	BT-19E	BT-36	NB02-120	NB02-159	BT-17-01	BT-33	BM-02	BM-03	BC-01	BC-02	BC-03
Description	granite	granitoid	granitoid	granitoid	granitoid	biotite gneiss	pegmatite	granite dike	grano-diorite	granite peg	granitoid	granitoid	granitoid
(wt. %)													
SiO_2	69.19	71.87	73.69	68.73	65.08	58.61	76.82	70.19	65.30	52.00	74.77	69.97	70.28
Al_2O_3	16.07	13.86	14.15	14.39	16.71	18.39	13.69	15.74	16.10	15.53	13.25	15.15	14.79
TiO_2	0.464	0.342	0.099	0.678	0.601	1.408	0.043	0.015	0.598	0.248	0.138	0.417	0.318
FeO	2.55	2.48	1.18	4.26	4.30	6.46	0.45	0.24	4.11	0.82	1.45	2.99	2.13
MnO	0.036	0.041	0.075	0.078	0.090	0.109	0.009	0.027	0.086	0.075	0.028	0.078	0.058
CaO	3.15	1.94	0.85	1.51	3.42	4.40	2.33	0.13	4.16	15.42	1.18	2.79	2.45
MgO	0.87	0.75	0.22	1.14	1.57	2.65	0.18	0.08	1.65	0.24	0.55	0.71	0.74
K_2O	2.58	4.83	5.21	4.99	3.58	3.02	1.39	9.72	2.85	0.35	1.54	3.03	3.38
Na_2O	4.04	2.64	3.79	3.00	3.48	3.30	4.72	1.98	3.92	8.18	5.41	4.06	4.13
P_2O_5	0.167	0.097	0.037	0.214	0.207	0.381	0.013	0.146	0.104	0.091	0.034	0.104	0.069
Total	99.11	98.85	99.30	98.99	99.04	98.73	99.65	98.27	98.87	92.95	98.35	99.30	98.35
(ppm)													
Ni	3	8	9	15	4	4	5	6	9	3	6	4	5
Cr	5	6	0	17	5	11	0	0	17	5	0	0	0
Sc	1	6	6	8	9	6	1	1	11	0	4	8	4
V	40	34	3	46	73	121	7	4	82	10	3	18	21
Ba	694	1000	64	257	1070	638	182	255	342	75	70	529	309
Rb	86	152	673	284	134	225	42	642	148	15	76	168	155
Sr	599	277	50	136	451	412	233	47	163	457	104	174	156
Zr	190	209	105	297	209	431	73	16	180	149	90	227	150
Y	13	33	112	43	23	18	15	9	31	36	24	25	20
Nb	7.8	14.2	64.0	51.1	12.1	27.3	10.6	3.1	12.9	19.0	11.3	14.4	10.6
Ga	21	16	18	24	21	23	20	18	18	13	14	15	17
Cu	5	2	0	4	5	0	9	0	11	0	0	3	0
Zn	63	43	34	69	76	102	30	11	50	7	12	49	37
Pb	22	27	50	23	20	15	12	79	19	6	5	12	13
La	35	44	34	84	49	18	18	9	51	40	28	56	43
Ce	80	94	59	161	101	56	56	8	74	93	37	99	48
Th	7	16	35	34	17	4	4	0	28	29	41	29	24
Y + Nb	21	47	176	94	35	45	26	12	44	55	35	39	31
Rb/Sr	0.144	0.549	13.460	2.088	0.297	0.546	0.180	0.016	0.908	0.033	0.731	0.966	0.994
A/CNK	**1.060**	**1.058**	**1.054**	**1.100**	**1.056**	**1.101**	**1.014**	**1.123**	**0.942**	**0.371**	**1.042**	**1.008**	**0.992**
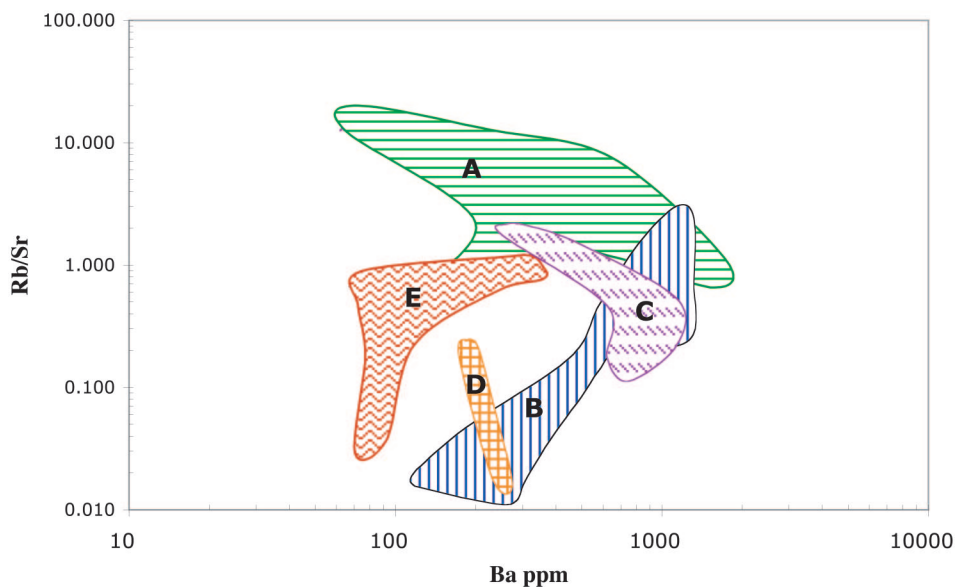
Fig. 12. Rb/Sr ratio vs. Ba (ppm) plot, showing the geochemical variation among sample groups. Fields labeled by geographic grouping: (A) Namche Barwa massif granitoids (green horizontal lines), (B) NW margin of NB-GP massif granites (blue vertical lines), (C) western Gangdese and related samples (purple diagonal dashes), (D) Northern granites (orange crosshatch pattern), and (E) northeastern/Bomi region granitoids (red wavy lines), data from table 2. Note the higher frequency of decompression melts (Rb/Sr ratios > 1.4) among the group A (Namche Barwa) granite suite.

extensively meteoric water has pervaded the crust; (4) the level of metamorphism previously experienced by rocks entering the massif—if they were low-grade and fertile, fluid-present melting would dominate, as opposed to Nanga Parbat, where rocks had undergone earlier high-grade metamorphism and were entering the massif relatively dry; or (5) deformation coeval with emplacement of melts, enhancing fluid infiltration—some samples show clear evidence of syn-kinematic emplacement and foliation.

     Tectonic discrimination of granites.—Southeastern Tibet is tectonically complex, but trace-element modeling provides constraints on the dominant tectonic regime that is reflected in the geochemistry of granitic melts. Trace-element geochemical analyses indicate that the majority of the granites are calc-alkaline to alkaline, plotting in the field of volcanic arc granites (fig. 13) of Pearce and others (1984) and in the "post"-collision granite field of Pearce (1996). Pearce (1996) emphasized that the collisional granites are the most difficult to classify on the basis of chemistry, as they have the greatest range of sources. Unlike granites from other settings, collisional granites cannot be explained and modeled by their trace element geochemical behavior, in terms of a single, well-defined mantle or crustal source. They can result from melting of the upper mantle due to adiabatic decompression that accompanies collisional uplift and erosion (England and Thompson, 1984), and might plot in either the volcanic arc or the within-plate field. In southeastern Tibet, volcanic arc activity is clearly present north of the Namche Barwa syntaxis, but within the massif itself the source of the melts is more ambiguous. Young zircon ages (<10 Ma) in the context of a 60 ± 10 Ma Himalayan orogeny require that these melts are not related to early thrusting and crustal thickening/shortening. The presence of decompression melts in a region that is being exhumed rapidly is also characteristic of later stages of collisional
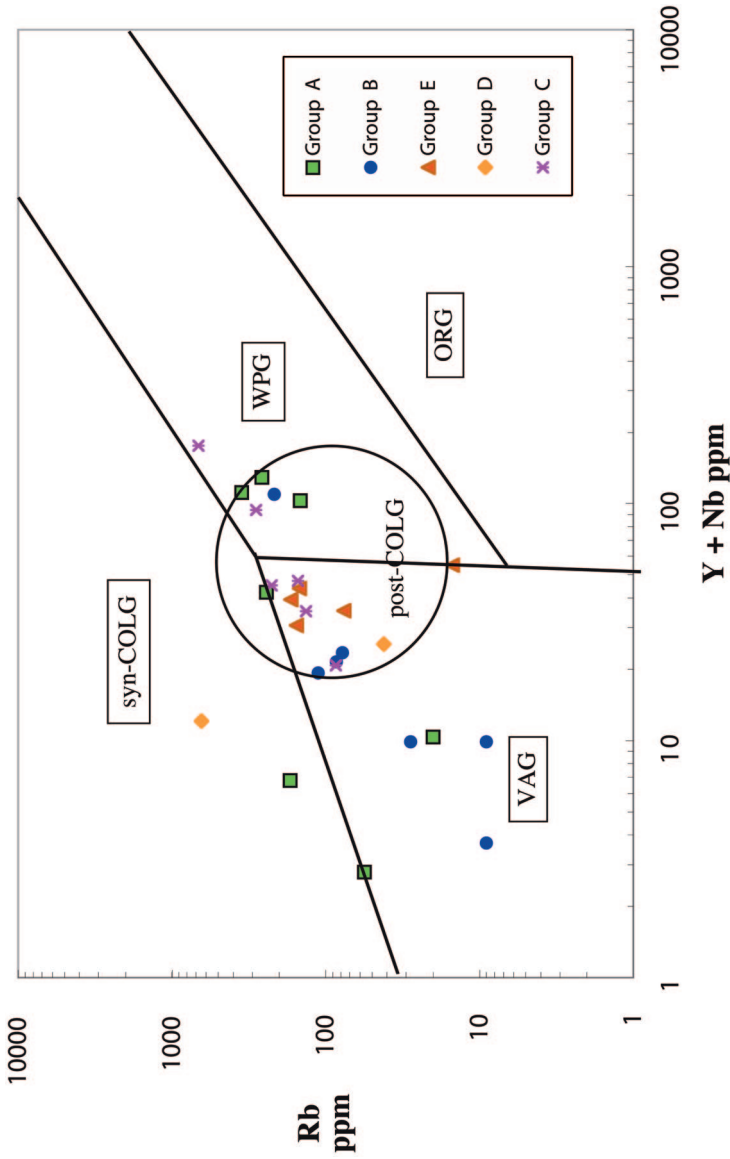
Fig. 13. Rb *vs.* Y + Nb diagram after Pearce and others (1984) and Pearce (1996) for granitoid groups: (A) Within the Namche Barwa massif (squares), (B) Northwest margin of NB-GP massif (circles), (C) Western Gangdese and related granites (asterisks), (D) north of NB-GP massif (diamonds), and (E) Northeastern/Bomi region (triangles). Syn-COLG and post-COLG: Syn- and "Post"-Collision Granites; WPG: Within Plate Granites; VAG: Volcanic Arc Granites; ORG: Ocean Ridge Granites.

tectonic settings. Hence, the distribution of Namche Barwa granites on Pearce and others' (1984) tectonic discrimination diagram, spanning the volcanic arc and within plate fields, is in accordance with our other data sets, specifically zircon ages, Rb/Sr geochemistry and geological and tectonic settings.

Zircon core ages provide further constraints on the source area for these granitoids. For group A samples, U-Pb ages of predominantly 400 to 500 Ma, with some 700 to 800 Ma ages (table 1) imply an Indian plate precursor for the youngest melts. Outside of Namche Barwa, most core ages are greater than 500 Ma, with the oldest protolith ages (0.9 - 2.4 Ga) present in the northern and western granite groups. Lhasa block material is the most likely source for these granites, but older metasediments or Indian continental basement cannot be ruled out on this basis alone.

<div align="center">DISCUSSION</div>

Namche Barwa granites.—The granites from Namche Barwa exhibit zircon U-Pb ages consistently under 10 Ma and thus are distinct from those reported elsewhere in the Himalayas. The young ages correspond to a period of rapid denudation at Namche Barwa, estimated at ∼10 mm/yr over the last 4 Myr (Burg and others, 1997). Coincidence of young granites with a period of rapid erosion suggests a cause-effect relationship, in particular a scenario involving decompression melting that mimics Nanga Parbat in the western Himalayan syntaxis. Relatively high Rb/Sr ratios in the Namche Barwa granites support a decompression melting regime similar to Nanga Parbat, where rapid exhumation has led to leucogranite emplacement by fluid-absent breakdown of muscovite (Zeitler and Chamberlain, 1991; Butler and others, 1997; Whittington and others, 1999). Young activity and decompression melts are evidence in favor of a "tectonic aneurysm" model (Zeitler and others, 2001a; Koons and others, 2002), attributing anatexis and high-grade metamorphism to rapid exhumation by the Yalu Tsangpo.

Coupled thermal-mechanical-erosional modeling (Koons and others, 1998; Zeitler and others, 2001b; Koons and others, 2002) shows that in a deforming orogen, local rheological variations will arise from deep and rapid incision. The crust will weaken as the strong upper crust is stripped from above by erosion and the local geotherm is steepened from below by rapid uplift of hot rock. If this process occurs where the crust is already weak, it will focus local upward movement of material from below. Provided that efficient erosion continues, a positive feedback develops in which flow of material into this weakened zone maintains local elevation and relief, reinforcing the concentrated exhumation and bowing up isotherms, further weakening the upper crust. This focusing of strain and rapid exhumation leads to metamorphic and structural overprinting of the crust as high-temperature lower crustal rocks are isothermally decompressed, and also leads to development of large mountains of limited spatial extent perched atop hot, weak crust. It is this concentration of exhumation and redirection of strain, with associated thermal, petrological, and geophysical anomalies, that Zeitler and others (2001a) dubbed a "tectonic aneurysm," in the sense of self-sustained failure of a normally strong boundary. Inherent in this model is the notion that feedback can amplify rather local geomorphic processes to the point where they exert a profound influence on the metamorphic and structural evolution of rocks at considerable depth. The emplacement of young melts near the core of Namche Barwa seems to support this model.

Granites outside Namche Barwa.—Zircon core and rim ages from the E-W transect across the western margin of Gyala Peri confirm the location of the suture zone between Indian and Asian plate components. Paralleling the trend of several other geological units and foliations, the attenuated suture wraps around just to the west of the Gyala Peri massif. West of Gyala Peri, U-Pb ages of samples intruding Lhasa Block basement exhibit a distinct cluster within 40 to 70 Ma, corresponding to Gangdese

plutonism. However, the younger (<26 Ma) group in this area must be associated with a more recent metamorphic event, possibly related to slip along the Gangdese thrust, slab break-off, or slab detachment. Neogene magmatism in the Gangdese belt is uncommon but has been identified in several places, with calc-alkaline magmatism of Gangdese geochemical affinity documented at 18 to 16 Ma in southwestern Tibet (Miller and others, 1999) and at 16 to 10 Ma in south-central Tibet (Coulon and others, 1986). Samples BT-4, NB-35-02, BT-15, and BT-17 all yield U-Pb zircon ages between 24 to 26 Ma, but do not exhibit a decompression melt signature and are therefore unlikely to be related to an eastward continuation of the STDS. These samples do, however, show volcanic arc affinity as per Pearce and others (1984) and might represent young Gangdese-related magmatism. Harrison and others (2000) proposed that a continuous process produced calc-alkaline Gangdese magmatism through the Tertiary, caused by an input of heat from the asthenosphere. Through such a mechanism, our 24 to 26 Ma granites could have been produced as collisional melts, representing continued subduction of Indian lithosphere (Chung and others, 2003). Alternatively, slab break-off of the subducting Indian continental margin, or slab detachment, whereby the mantle lithosphere peels off from the overlying crust and passively sinks into the asthenosphere, might explain the origin of these magmas. Yet another possibility is that processes related to underthrusting on the Gangdese Thrust structure, such as dewatering or shear heating, contributed to production of these ~25 Ma granites.

The two 21 Ma samples from north of Namche Barwa (BT-33, BT-17) along the Jiali fault zone are distinct from the 24 to 26 Ma group north and west of Gyala Peri, based on their tectonic setting and geochemistry. These granites might be related to Miocene shearing as reported for the Red River fault (Schärer and others, 1990, 1994; Harrison and others, 1992; Leloup and Kienast, 1993; Leloup and others, 1993, 1995). Although the Red River fault is located considerably southeast of the eastern Himalayan syntaxis, it was at that time a left-lateral fault, possibly related to the ductile sinistral shear seen near Tungmai on the Jiali fault zone. An eastern extension of the Jiali-Parlung fault is reported to have been dextrally active during ~18 to 12 Ma (Lee and others, 2003), and perhaps the associated shear produced the 21 Ma granites that we observe. Common syntectonic emplacement of granitic melts in ductile strike-slip shear zones can be explained by partial melting of the lower crust, induced by shear heating in the upper mantle (for example, Leloup and others, 1999). If this is the case, samples BT-33 and BT-17 represent westward manifestations of the early Miocene oblique-slip tectonics and shear heating regime more prominent in easterly parts of the Tibetan-Himalayan orogen.

Another possible cause of Oligo-Miocene igneous activity in southern Tibet suggested by Yin (2000) is lithospheric-scale rifting, whereby large, deep cracks in the mantle lithosphere allow asthenosphere to flow upward, providing the necessary heat for melt production. Alternatively, the ~21 Ma granites could be related to slab break-off, slab detachment, or a Gangdese Thrust event, similar to the 24 to 26 Ma granites further southeast.

<div align="center">CONCLUSION</div>

Our U-Pb SHRIMP ages establish a complex tectonic history for southeastern Tibet, with the presence of at least five magmatic episodes: 400 to 500 Ma, ~120 Ma, 40 to 70 Ma, 18 to 25 Ma, and 3 to 10 Ma. The oldest age group is attributed to early Paleozoic tectonism. Later melting episodes are primarily related to the Cretaceous-Tertiary India-Asia convergence and collision, including the subduction of Neo-Tethys oceanic crust and Gangdese plutonism. Less expected, however, is the widespread occurrence of 20 to 25 Ma granitoids in the areas surrounding the Namche Barwa massif. These could be a product of slab break-off, slab delamination, Gangdese

thrusting, or early Miocene shearing accompanying dextral motion along the Jiali fault.

The youngest group (3 - 10 Ma) of granitoids, present within the core of the Namche Barwa massif along and near the Yalu Tsangpo gorge, provides solid evidence for a tectonic-surficial feedback relationship at Namche Barwa. Geochemical data indicates the presence of young granites produced by both fluid-absent and fluid-present melting in the Namche Barwa and adjacent regions, with a decompression melting regime dominating in the core of the Namche Barwa massif. Taken together, our geochronologic and geochemical data appear to support a tectonic aneurysm model for the development of Namche Barwa. Surrounding the Namche Barwa-Gyala Peri massif, however, granite emplacement results from distinctly different modes of production. This mode of production reflects the complex deformation at the eastern edge of the Indian plate, and the recent (Miocene and younger) activity along warped eastward expressions of dominant Himalayan structures.

REFERENCES

Aitchison, J. C., Davis, A. M., Badengzhu, and Luo, H., 2003, The Gangdese thrust: a phantom structure that did not raise Tibet: Terra Nova, v. 15, p. 155-162.
Blundy, J. D., and Wood, B. J., 1991, Crystal-chemical controls on the partitioning of Sr and Ba between plagioclase feldspar, silicate melts, and hydrothermal solutions: Geochimica et Cosmochimica Acta, v. 55, p. 193-209.
Burchfiel, B. C., King, R., Royden, L. H., Wang, E., Chen, Z., Zhang, X., and Zhao, J., 1998, Tectonic interpretation of GPS results from the SE part of the Tibetan Plateau and within the European/Asian framework: Abstracts with Programs - Geological Society of America, v. 30, p. 108.
Burg, J. P., Davy, P., Nievergelt, P., Oberli, F., Seward, D., Diao, Z., and Meier, M., 1997, Exhumation during crustal folding in the Namche Barwa syntaxis: Terra Nova, v. 9, p. 53-56.
Burg, J. P., Nievergelt, P., Oberli, F., Seward, D., Davy, P., Maurin, J. C., Diao, Z., and Meier, M., 1998, The Namche-Barwa syntaxis: Evidence for exhumation related to compressional crustal folding: Journal of Asian Earth Sciences, v. 16, p. 239-252.
Butler, R. W. H., Harris, N. B. W., and Whittington, A. G., 1997, Interactions between deformation, magmatism and hydrothermal activity during active crustal thickening: a field example from Nanga Parbat, Pakistan Himalayas: Mineralogical Magazine, v. 61, p. 37-52.
Chemenda, A. I., Burg, J. P., and Mattauer, M., 2000, Evolutionary model of the Himalaya–Tibet system: geopoem: based on new modelling, geological and geophysical data: Earth and Planetary Science Letters, v. 174, p. 397-409.
Chung, S. L., Lo, C. H., Lee, T. Y., Yuquan, Z., Yingwen, X., Xianhua, L., Wang, K. L., Wang, P. L., 1998, Diachronous uplift of the Tibet Plateau starting 40 Myr ago: Nature, v. 394, p. 769-773.
Chung, S. L., Liu, D., Ji, J., Chu, M. F., Lee, H. Y., Wen, D. J., Lo, C. H., Lee, T. Y., Qian, Q., and Zhang, Q., 2003, Adakites from continental collision zones: Melting of thickened lower crust beneath southern Tibet: Geology, v. 31, p. 1021-1024.
Copeland, P., Harrison, T. M., Yun, P., Kidd, W. S. F., Roden, M., and Zhang, Y., 1995, Thermal evolution of the Gangdese Batholith, southern Tibet; a history of episodic unroofing: Tectonics, v. 14, p. 223-236.
Coulon, C., Maluski, H., Bollinger, C., and Wang, S., 1986, Mesozoic and Cenozoic volcanic rocks from central and southern Tibet; ^{39}Ar-^{40}Ar dating, petrological characteristics and geodynamical significance: Earth and Planetary Science Letters, v. 79, p. 281-302.
DeCelles, P. G., Gehrels, G. E., Quade, J., Ojha, T. P., Kapp, P. A., and Upreti, B. N., 1998, Neogene foreland basin deposits, erosional unroofing, and the kinematic history of the Himalayan fold-thrust belt, western Nepal: Geological Society of America Bulletin, v. 110, p. 2-21.
DeCelles, P. G., Gehrels, G. E., Quade, J., LaReau, B., and Spurlin, M., 2000, Tectonic implications of U-Pb zircon ages of the Himalayan orogenic belt in Nepal: Science, v. 288, p. 497-499.
Debon, F., Zimmerman, J., Liu, G. H., Jin, C. W., and Xu, R. H., 1985, Time relationship between magmatism, tectonics and metamorphism in southern Tibet: new K-Ar data: Geology Rundsch, v. 74, p. 229-236.

Debon, F., Le Fort, P., Sheppard, S. M. F., and Sonet, J., 1986, The four plutonic belts of the Transhimalaya-Himalaya; a chemical, mineralogical, isotopic, and chronological synthesis along a Tibet-Nepal section: Journal of Petrology, v. 27, p. 219-250.

Dewey, J. F., Shackleton, R. M., Chengfa, C., and Yiyin, S., 1988, The tectonic evolution of the Tibetan Plateau: Philosophical Transactions of the Royal Society of London, Series A: Mathematical and Physical Sciences, v. 327, p. 379-413.

Ding, L., Zhong, D., Yin, A., Kapp, P., and Harrison, T. M., 2001, Cenozoic structural and metamorphic evolution of the eastern Himalayan syntaxis (Namche Barwa): Earth and Planetary Science Letters, v. 192, p. 423-438.

Ding, L., Kapp, P., Zhong, D., and Deng, W., 2003, Cenozoic Volcanism in Tibet: Evidence for a Transition from Oceanic to Continental Subduction: Journal of Petrology, v. 44, p. 1833-1865.

Edwards, M. A., and Harrison, T. M., 1997, When did the roof collapse? Late Miocene north-south extension in the high Himalaya revealed by Th-Pb monazite dating of the Khula Kangri Granite: Geology, v. 25, p. 543-546.

England, P. C., and Thompson, A. B., 1984, Pressure-temperature-time paths of regional metamorphism; II, Their inference and interpretation using mineral assemblages in metamorphic rocks: Journal of Petrology, v. 25, p. 929-955.

Ferrara, G., Lombardo, B., and Tonarini, S., 1983, Rb/Sr geochronology of granites and gneisses from the Mount Everest region, Nepal Himalaya: Geologische Rundschau, v. 72, p. 119-136.

Fielding, E., 1996, Tibet uplift and erosion: Tectonophysics, v. 260, p. 55-84.

Gehrels, G. E., DeCelles, P. G., Martin, A., Ojha, T. P., and Pinhassi, G., 2003, Initiation of the Himalayan orogen as an early Paleozoic thin-skinned thrust belt: GSA Today, v. 13, p. 4-9.

Geng, Q., Zheng, L., Pan, G., Ou, C., Sun, Z., Dong, H., Wang, X., Liu, Y., and Li, S., 2002, Ophiolitic Melanges in the Yarlung-Tsangpo "Big Bend" Canyon, SE Tibet: EOS, Transactions of the American Geophysical Union, v. 83, p. T51B-1145.

Hallet, B., and Molnar, P., 2001, Distorted drainage basins as markers of crustal strain east of the Himalaya: Journal of Geophysical Research, v. 106, p. 13,697-13,709.

Harris, N. B. W., and Inger, S., 1992, Trace element modelling of pelite-derived granites: Contributions to Mineralogy and Petrology, v. 110, p. 46-56.

Harris, N. B. W., and Massey, J., 1994, Decompression and anatexis of Himalayan metapelites: Tectonics, v. 13, p. 1537-1546.

Harris, N. B. W., Inger, S., and Massey, J., 1993, The role of fluids in the formation of High Himalayan leucogranites, *in* Treloar, P. J., and Searle, M. P., Himalayan tectonics: Geological Society Special Publications, v. 74, p. 391-400.

Harrison, T. M., Copeland, P., Kidd, W. S. F., and Yin, A., 1992, Raising Tibet: Science, v. 255, p. 1663-1670.

Harrison, T. M., Ryerson, F. J., Le Fort, P., Yin, A., Lovera, O. M., and Catlos, E. J., 1997a, A Late Miocene-Pliocene origin for the Central Himalayan inverted metamorphism: Earth and Planetary Science Letters, v. 146, p. E1-E7.

Harrison, T. M., Lovera, O. M., and Grove, M., 1997b, New insights into the origin of two contrasting Himalayan granite belts: Geology, v. 25, p. 899-902.

Harrison, T. M., Grove, M., Lovera, O. M., and Catlos, E. J., 1998, A model for the origin of Himalayan anatexis and inverted metamorphism: Journal of Geophysical Research, v. 103, p. 27,017-27,032.

Harrison, T. M., Yin, A., Grove, M., Lovera, O. M., Ryerson, F. J., and Xinhua, Z., 2000, The Zedong Window; a record of superposed Tertiary convergence in southeastern Tibet: Journal of Geophysical Research, v. 105, p. 19,211-19,230.

Hodges, K. V., 2000, Tectonics of the Himalaya and southern Tibet from two perspectives: GSA Bulletin, v. 112, p. 324-350.

Hodges, K. V., Parrish, R. R., Housh, T. B., Lux, D. R., Burchfiel, B. C., Royden, L. H., and Chen, Z., 1992, Simultaneous Miocene extension and shortening in the Himalayan Orogen: Science, v. 258, p. 1466-1470.

Hodges, K. V., Parrish, R. R., and Searle, M. P., 1996, Tectonic evolution of the central Annapurna Range, Nepalese Himalayas: Tectonics, v. 15, p. 1264-1291.

Kapp, P., Murphy, M. A., Yin, A., Harrison, T. M., Ding, L., and Guo, J., 2003a, Mesozoic and Cenozoic tectonic evolution of the Shiquanhe area of western Tibet: Tectonics, v. 22, no. 4, 1029, doi:10.1029/2001TC001332.

Kapp, P., Yin, A., Manning, C. E., Harrison, T. M., Taylor, M. H., and Ding, L., 2003b, Tectonic evolution of the early Mesozoic blueschist-bearing Qiangtang metamorphic belt, central Tibet: Tectonics, v. 22, no. 4, 1043, doi:10.1029/2002TC001383.

Kohn, M. J., and Parkinson, C. D., 2002, Petrologic case for Eocene slab breakoff during the Indo-Asian collision: Geology, v. 30, p. 591-594.

Koons, P. O., Craw, D., Cox, S. C., Upton, P., Templeton, A. S., and Chamberlain, C. P., 1998, Fluid flow during active oblique convergence; a Southern Alps model from mechanical and geochemical observations: Geology, v. 26, p. 159-162.

Koons, P. O., Zeitler, P. K., Chamberlain, C. P., Craw, D., and Meltzer, A. S., 2002, Mechanical links between erosion and metamorphism in Nanga Parbat, Pakistan Himalaya: American Journal of Science, v. 302, p. 749-773.

Kosarev, G., Kind, R., Sobolev, S. V., Yuan, X., Hanka, W., and Oreshin, S., 1999, Seismic evidence for a detached Indian lithospheric mantle beneath Tibet: Science, v. 283, p. 1306-1309.

Lee, H. Y., Chung, S. L., Wang, J. R., Wen, D. J., Lo, C. H., Yang, T. F., Zhang, Y., Xie, Y., Lee, T. Y., Wu, G., and Ji, J., 2003, Miocene Jiali faulting and its implications for Tibetan tectonic evolution: Earth and Planetary Science Letters, v. 205, p. 185-194.

Le Fort, P., 1975, Himalaya: the collided range. Present knowledge of the continental arc: American Journal of Science, v. 275, p. 1-44.

——— 1981, Manaslu leucogranite: A collision signature of the Himalaya, a model for its genesis and emplacement: Journal of Geophysical Research, v. 86, p. 10545-10568.

Le Fort, P., Debon, F., and Sunet, J., 1980, The "Lesser Himalayan" cordierite granite belt, typology and age of the pluton of Manserah (Pakistan), *in* Tahirkheli, R. A. K., Jan, M. Q., and Majid, M., editors, Proceedings of the International Committee on Geodynamics Group 6 meeting: Geological Bulletin, University of Peshawar special issue, v. 13, p. 51-61.

Le Fort, P., Debon, F., Pecher, A., Sonet, J., and Vidal, P., 1986, The 500 Ma magmatic event in Alpine southern Asia, a thermal episode at Gondwana Scale: Sciences de la Terre, Mémoires, v. 47, p. 191-209.

Le Fort, P., Cuney, M., Deniel, C., France-Lanord, C., Sheppard, S. M. F., Upreti, B. N., and Vidal, P., 1987, Crustal generation of the Himalayan leucogranites: Tectonophysics, v. 134, p. 39-57.

Leloup, P. H., and Kienast, J. R., 1993, High-temperature metamorphism in a major strike-slip shear zone; the Ailao Shan-Red River, People's Republic of China: Earth and Planetary Science Letters, v. 118, p. 213-234.

Leloup, P. H., Harrison, T. M., Ryerson, F. J., Wenji, Chen, Qi, Li, Tapponnier, P., and Lacassin, R., 1993, Structural, petrological and thermal evolution of a Tertiary ductile strike-slip shear zone, Diancang Shan, Yunnan: Journal of Geophysical Research, v. 98, p. 6715-6743.

Leloup, P. H., Lacassin, R., Tapponnier, P., Schaerer, U., Z. Dalai, L. Xiaohan, Zhang, L., J. Shaocheng, and Trinh, P. T., 1995, The Ailao Shan-Red River shear zone (Yunnan, China), Tertiary transform boundary of Indochina: Tectonophysics, v. 251, p. 3-84.

Leloup, P. H., Ricard, Y., Battaglia, J., and Lacassin, R., 1999, Shear heating in continental strike-slip shear zones; model and field examples: Geophysical Journal International, v. 136, p. 19-40.

Liu, Y., and Zhong, D., 1997, Petrology of high-pressure granulites from the eastern Himalayan syntaxis: Journal of Metamorphic Geology, v. 15, p. 451-466.

Ludwig, K. R., 2001, User's Manual for Isoplot/Ex, Version 2.49, A Geochronological Toolkit for Microsoft Excel: Berkeley Geochronology Center Special Publication No. 1a, 55 p.

Maheo, G., Guillot, S., Blichert-Toft, J., Rolland, Y., and Pecher, A., 2002, A slab breakoff model for the Neogene thermal evolution of South Karakorum and South Tibet: Earth and Planetary Science Letters, v. 195, p. 45-58.

Maluski, H., Matte, P., and Brunel, M., 1988, Argon 39-Argon 40 dating of metamorphic and plutonic events in the North and High Himalaya belts (southern Tibet-China): Tectonics, v. 7, p. 299-326.

Meyer, B., Tapponnier, T., Bourjot, L., Metivier, F., Gaudemer, Y., Peltzer, G., Shunmin, G., and Zhitai, C., 1998, Crustal thickening in Gansu-Qinghai, lithospheric mantle subduction, and oblique, strike-slip controlled growth of the Tibet Plateau: Geophysical Journal International, v. 135, p. 1-47.

Miller, C., Schuster, R., Kloetzli, U. S., and Frank, W., 1999, Purtscheller, F., Post-collisional potassic and ultrapotassic magmatism in SW Tibet; geochemical and Sr-Nd-Pb-O isotopic constraints for mantle source characteristics and petrogenesis: Journal of Petrology, v. 40, p. 1399-1424.

Miller, C., Thoni, M., Frank, W., Grazemann, B., Kloetzli, U. S., Guntli, P., and Dragnitis, E., 2001, The early Paleozoic magmatic event in the northwest Himalaya, India: source, tectonic setting and age of emplacement: Geological Magazine, v. 138, p. 237-251.

Molnar, P., England, P., and Martinod, J., 1993, Mantle dynamics, the uplift of the Tibetan plateau, and the Indian monsoon: Reviews of Geophysics, v. 31, p. 357-396.

Murphy, M. A., and Harrison, T. M., 1999, Relationship between leucogranites and the Qomolangma detachment in the Rongbuk Valley, south Tibet: Geology, v. 27, p. 831-834.

Murphy, M. A., and Yin, A., 2003, Structural evolution and sequence of thrusting in the Tethyan fold-thrust belt and Indus-Yalu suture zone, southwest Tibet: Geological Society of America Bulletin, v. 115, p. 21-34.

Murphy, M. A., Yin, A., Harrison, T. M., Dürr, S. B., Chen, Z., Ryerson, F. J., Kidd, W. S. F., Wang, X., and Zhou, X., 1997, Did the Indo-Asian collision alone create the Tibetan plateau?: Geology, v. 25, p. 719-722.

Nash, W. P., and Crecraft, H. R., 1985, Partition coefficients for trace elements in silicic magmas: Geochimica et Cosmochimica Acta, v. 49, p. 2309-2322.

Pearce, J. A., 1996, A user's guide to basalt discrimination diagrams, *in* Wyman, D. A., editors, Trace Element Geochemistry of Volcanic Rocks: Applications for Massive Sulphide Exploration: Geological Association of Canada, Short Course Notes v. 12, p. 79-113.

Pearce, J. A., Harris, N., and Tindle, A., 1984, Trace element discrimination diagrams for the tectonic interpretation of granitic rocks: Journal of Petrology, v. 25, p. 956-983.

Quidelleur, X., Grove, M., Lovera, O. M., Harrison, T. M., Yin, A., and Ryerson, F. J., 1997, Thermal evolution and slip history of the Renbu Zedong Thrust, southeastern Tibet: Journal of Geophysical Research, v. 102, p. 2659-2679.

Ratschbacher, L., Frisch, W., Liu, G., and Chen, C. C., 1994, Distributed deformation in southern and western Tibet during and after the India-Asia collision: Journal of Geophysical Research, v. 99, p. 19,917-19,945.

Scaillet, B., Pecher, A., Rochette, P., and Champenois, M., 1995, The Gangotri granite (Garhwal Himalaya): laccolith emplacement in an extending collisional belt: Journal of Geophysical Research, v. 100, p. 585-607.

Schärer, U., Xu, R. H., and Allegre, C. J., 1984, U-Pb geochronology of Gangdese (Transhimalaya) plutonism in the Lhasa-Xigaze region, Tibet: Earth and Planetary Science Letters, v. 69, p. 311-320.

Schärer, U., Tapponnier, P., Lacassin, R., Leloup, P. H., Zhong Dalai, and Ji, S., 1990, Intraplate tectonics in Asia: A precise age for large-scale Miocene movement along the Ailao Shan – Red River shear zone, China: Earth and Planetary Science Letters, v. 97, p. 65-77.

Schärer, U., Zhang L.S., and Tapponnier, P., 1994, Duration of strike-slip movements in large shear zones: The Red River belt, China: Earth and Planetary Science Letters, v. 126, p. 379-397.

Stacey, J. S., and Kramers, J. D., 1975, Approximation of terrestrial lead isotopic evolution by a two-stage model: Earth and Planetary Science Letters, v. 26, p. 207-221.

Tilmann, F., Ni, J., Hearn, T., Ma, Y. S., Rapine, R., Kind, R., Mechie, J., Saul, J., Haines, S., Klemperer, S., Brown, L., Pananont, P., Ross, A., Nelson, K. D., Guo, J., and Zhao, W., 2003, Seismic imaging of the downwelling Indian lithosphere beneath central Tibet: Science, v. 300, p. 1424-1427.

Trivedi, J. R., Gopalan, K., and Valdiya, K. S., 1984, Rb-Sr ages of granitic rocks within the Lesser Himalayan nappes, Kumaun, India: Journal of the Geological Society of India, v. 25, p. 641-654.

Turner, S., Arnaud, N., Liu, J., Rogers, N., Hawkesworth, C., Harris, N., Kelley, S., van Calsteren, P., and Deng, W., 1996, Postcollision, shoshonitic volcanism on the Tibetan Plateau: Implications for convective thinning of the lithosphere and the source of ocean island basalts: Journal of Petrology, v. 37, p. 45-71.

Wang, E., and Burchfiel, B. C., 1997, Interpretation of Cenozoic tectonics in the right-lateral accommodation zone between the Ailao Shan shear zone and the eastern Himalayan syntaxis: International Geology Review, v. 39, p. 191-219.

Wang, J., Yin, A., Harrison, T. M., Grove, M., Yuquan, Z., and Guanghong, X., 2001, A tectonic model for Cenozoic igneous activities in the eastern Indo-Asian collision zone: Earth and Planetary Science Letters, v. 188, p. 123-133.

Whittington, A. G., and Treloar, P. J., 2002, Crustal anatexis and its relation to the exhumation of collisional orogenic belts, with particular reference to the Himalaya: Mineralogical Magazine, v. 66, p. 53-91.

Whittington, A. G., Harris, N. B. W., and Butler, R. W. H., 1999, Contrasting anatectic styles at Nanga Parbat, northern Pakistan, *in* Macfarlane, A., Sorkhabi, R. B., and Quade, J., editors, Himalaya and Tibet; mountain roots to mountain tops: Boulder, Colorado, Geological Society of America Special Paper, v. 328, p. 129-144.

Williams, H., Turner, S., Kelley, S., and Harris, N., 2001, Age and composition of dikes in southern Tibet: New constraints on the timing of east-west extension and its relationship to postcollisional magmatism: Geology, v. 29, p. 339-342.

Williams, I. S., 1998, U-Th-Pb Geochronology by Ion Microprobe, *in* McKibben, M. A., Shanks III, W. C., and Ridley, W. I., editors, Applications of Microanalytical Techniques to Understanding Mineralizing Processes: Society of Economic Geologists, review v. 7, p. 1-35.

Winslow, D. M., Chamberlain, C. P., and Zeitler, P. K., 1995, Metamorphism and melting of the lithosphere due to rapid denudation, Nanga Parbat Massif, Himalaya: Journal of Geology, v. 103, p. 395-409.

Yin, A., 2000, Mode of Cenozoic east-west extension in Tibet suggesting a common origin of rifts in Asia during the Indo-Asian collision: Journal of Geophysical Research, B, Solid Earth and Planets, v. 105, p. 21,745-21,759.

Yin, A., and Harrison, T. M., 2000, Geologic evolution of the Himalayan-Tibetan orogen: Annual Review of Earth and Planetary Sciences, v. 28, p. 211-280.

Yin, A., Harrison, T. M., Ryerson, F. J., Chen, W., Kidd, W. S. F., and Copeland, P., 1994, Tertiary structural evolution of the Gangdese thrust system, southwestern Tibet: Journal of Geophysical Research, v. 99, p. 18,175-18,201.

Yin, A., Harrison, T. M., Murphy, M. A., Grove, M., Nie, S., Ryerson, F. J., Feng, W. X., and Le, C. Z., 1999, Tertiary deformation history of southeastern and southwestern Tibet during the Indo-Asian collision: Geological Society of America Bulletin, v. 111, p. 1644-1664.

Zeitler, P. K., and Chamberlain, C. P., 1991, Petrogenetic and tectonic significance of young leucogranites from the NW Himalaya, Pakistan: Tectonics, v. 10, p. 729-741.

Zeitler, P. K., Chamberlain, C. P., and Smith, H., 1993, Synchronous anatexis, metamorphism, and rapid denudation at Nanga Parbat, Pakistan Himalaya: Geology, v. 21, p. 347-350.

Zeitler, P. K., Meltzer, A. S., Koons, P. O., Craw, D., Hallet, B., Chamberlain, C. P., Kidd, W. S. F., Park, S. K., Seeber, L., Bishop, M., and Shroder, J., 2001a, Erosion, Himalayan geodynamics, and the geomorphology of metamorphism: GSA Today, 11, p. 4-8.

Zeitler, P. K., Koons, P. O., Bishop, M. P., Chamberlain, C. P., Craw, D., Edwards, M. A., Hamidullah, S., Jan, M. Q., Khan, M., Khattak, M., Kidd, W. S. F., Mackie, R. L., Meltzer, A. S., Park, S. K., Pecher, A., Poage, M. A., Sarker, G., Schneider, D. A., Seeber, L., and Shroder, J. F., 2001b, Crustal reworking at Nanga Parbat, Pakistan; metamorphic consequences of thermal-mechanical coupling facilitated by erosion: Tectonics, v. 20, p. 712-728.

Zhang, L. S., and Schärer, U., 1999, Age and origin of magmatism along the Cenozoic Red River shear belt, China: Contributions to Mineralogy and Petrology, v. 134, p. 67-85.

Zhang, Z. G., Liu, Y. H., Qnag, H. X., and Xu, B. C., 1992, Geology of the Namche Barwa Region: Beijing, Chinese Science Press, 185 p.